GEOSPHERE

GEOSPHERE

https://doi.org/10.1130/GES02634.1

12 figures; 2 tables; 1 set of supplemental files

CORRESPONDENCE: lydiabailey@fas.harvard.edu

CITATION: Bailey, L.R., Reiners, P.W., Ferguson, G., McIntosh, J., Kim, J.-H., and Hemming, S., 2024, Pliocene subsurface fluid flow driven by rapid erosional exhumation of the Colorado Plateau, southwestern USA: Geosphere, /10.1130/GES02634.1.

Science Editor: Christopher J. Spencer Associate Editor: Gregory D. Hoke

Received 22 December 2022 Revision received 20 November 2023 Accepted 21 December 2023

Published online 8 March 2024





This paper is published under the terms of the CC-BY-NC license

© 2024 The Authors

Pliocene subsurface fluid flow driven by rapid erosional exhumation of the Colorado Plateau, southwestern USA

Lydia R. Bailey^{1,*}, Peter W. Reiners¹, Grant Ferguson^{2,3}, Jennifer McIntosh³, Ji-Hyun Kim⁴, and Sidney Hemming⁵

- ¹Department of Geosciences, University of Arizona, Tucson, Arizona 85721, USA
- ²Department of Hydrology and Atmospheric Sciences, University of Arizona, Tucson, Arizona 85721, USA
- ³Department of Civil, Geological and Environmental Engineering, University of Saskatchewan, Saskatoon, SK S7N 5A9, Canada
- ⁴Department of Geosciences, University of Calgary, Calgary, AB T2N 1N4, Canada
- ⁵Lamont-Doherty Earth Observatory, Columbia University, Palisades, New York 10954, USA

ABSTRACT

Erosion may modify the architecture of subsurface flow systems by removing confining units and changing topography to influence patterns of fluid circulation or by inducing gas exsolution from subsurface fluids, influencing compositional and buoyancy patterns in flow systems. Here, we examine the geologic record of subsurface flow in the sedimentary rocks of the Paradox Basin in the Colorado Plateau (southwestern USA), including the distribution and ages of Fe- and Mn-oxide deposits and bleached, former red-bed sandstones. We compare our results to those of previous geo- and thermochronology studies that documented as much as 2 km of erosional exhumation at ca. 3-4 Ma and Fe-and Mn-oxide precipitation at 3.6 Ma along fault zones in the region.

We used (U-Th)/He and K-Ar dating to document two new records of subsurface flow of reduced fluids between 3 and 4 Ma. The first is precipitation of Mn-oxides along the Moab fault (Utah, USA) at 3.9 ± 0.2 Ma. The second is clay mineralization associated with laterally extensive bleaching in the Curtis Formation, which we dated using K-Ar illite age analysis to 3.60 ± 0.03 Ma. The coincidence of the timing of bleaching, Fe- and Mn-oxide formation in multiple locations, and erosional exhumation at 3-4 Ma raises the question of how surface erosion may have induced a phase of fluid flow in the subsurface. We suggest that recent erosion of the Colorado Plateau created steep topographic gradients that enhanced regional groundwater flow, whereby meteoric water circulation flushed reduced fluids toward discharge zones. Dissolved gases, transported from hydrocarbon reservoirs, also may have been exsolved by rapid depressurization.

Lydia Ruth Bailey https://orcid.org/0000-0003-1393-7911

INTRODUCTION

The configuration, chemistry, and fluxes of basinal flow systems are determined by topography (Tóth, 1963; Haitjema and Mitchell-Bruker, 2005), stratigraphy (or subsurface architecture) (Freeze and Witherspoon, 1967; Tóth, 1970), climate (Salvucci and Entekhabi, 1995; Maxwell and Kollet, 2008) as well as tectonic regimes (Vrolijk, 1987; Garven, 1995; Koons et al., 1998; McLellan et al., 2004; Cui et al., 2012), subsidence (Bethke, 1985; Bjørlykke and Høeg, 1997; Bjørlykke, 1999), and fluid density contrasts (Ranganathan and Hanor, 1988; Fan et al., 1997; Adams and Bachu, 2002; Ferguson et al., 2018). Topography is one of the major driving forces for groundwater flow, and therefore, the erosional evolution of sedimentary basins can transiently influence patterns and extents of fluid transport in regional-scale flow systems (Adams et al., 2004). Greater topographic relief is associated with a deeper extent of meteoric water circulation (McIntosh and Ferguson, 2021), increased recharge, and increased export of groundwater to surface water bodies (Salvucci and Entekhabi, 1995; Marklund and Wörman, 2007). Erosion and subsequent exhumation can also cause a decrease in subsurface pressure and temperature, which decreases the solubility, and causes exsolution, of dissolved gases (Cramer et al., 2002). Heterogeneity in the porosity and permeability distribution of the geologic framework can modify the configuration of subsurface flow systems, intensity of vertical and horizontal flow components, and relative extents of recharge and discharge areas (Tóth, 1970). The chemical composition of subsurface fluids is also controlled by geology. Fluids dissolve soluble minerals in the rock matrix, and with continued interaction, the chemical composition of the fluids evolve from bicarbonate-dominated through to sulfate- or chloride-dominated water, for example (Freeze and Cherry, 1979; Tóth, 1999).

The Colorado Plateau of the southwestern United States (Fig. 1) hosts a diverse variety of subsurface fluids such as widespread hydrocarbon, CO2, and He accumulations, fresh and brackish groundwater, and hydrothermal, magmatic, and mantle-derived fluids. The Colorado Plateau also has a dynamic history of deposition and denudation that has altered the permeability distribution and topographic gradients, likely changing the subsurface fluid flow

^{*}Now at Department of Earth and Planetary Sciences, Harvard University, Cambridge, Massa chusetts 02138, USA

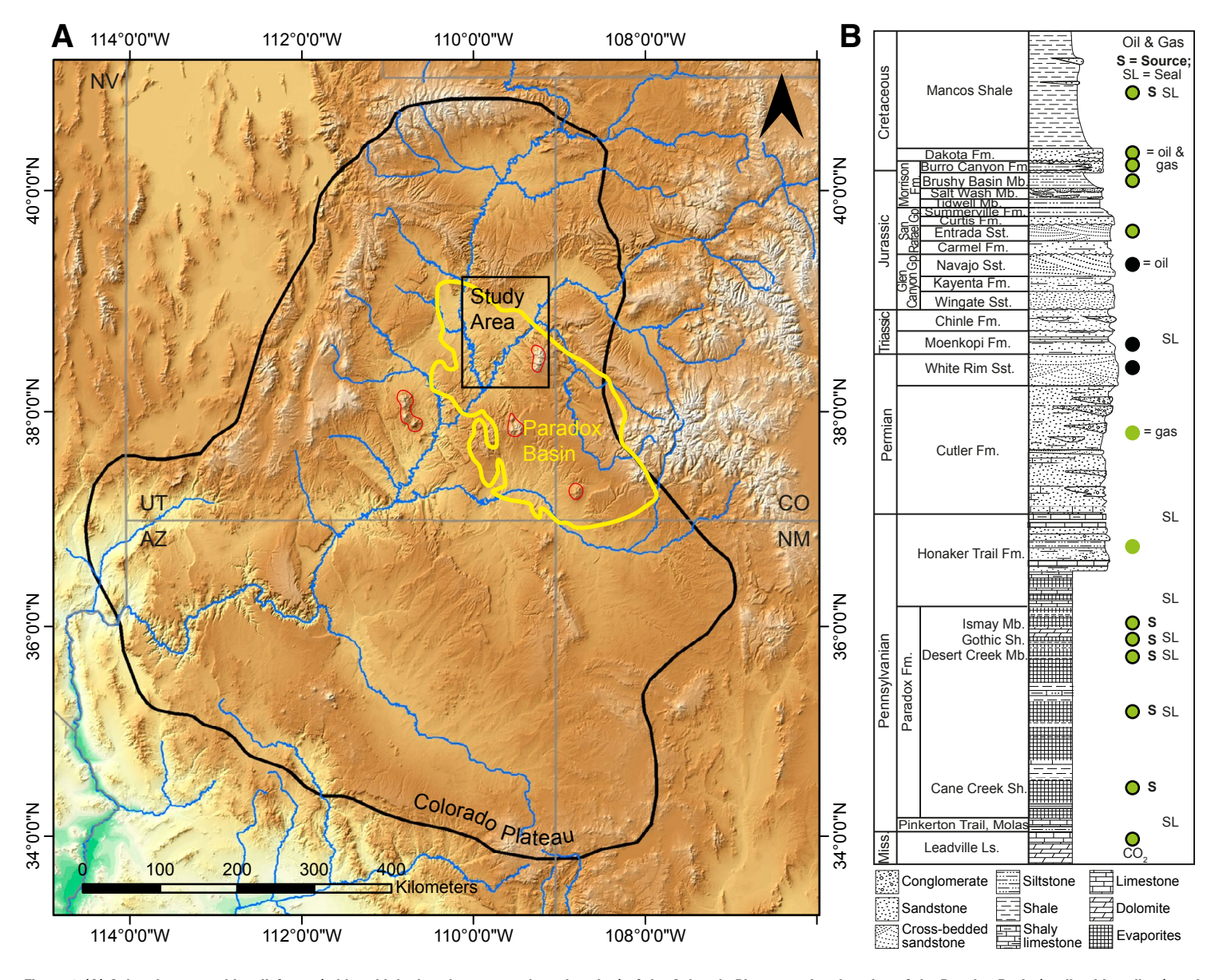


Figure 1. (A) Colored topographic relief map (white—high elevation; green—low elevation) of the Colorado Plateau region, location of the Paradox Basin (outlined in yellow), and location of the study area. Major river networks are in blue, and Oligocene-aged laccolith intrusions are outlined in red. CO—Colorado; NM—New Mexico; AZ—Arizona; UT—Utah; NV—Nevada. (B) Stratigraphic column for the Paradox Basin with the stratigraphic locations of oil and gas reservoirs. S—source rock; SL—seal rock; green circle—gas reservoir; black circle—oil reservoir; black and green circle—oil and gas reservoir; CO₂—CO₂ reservoir; Fm.—Formation; Gp—Group; Mb.—Member; Sst.—Sandstone; Sh.—Shale; Ls.—Limestone.

systems through time. For example, Tyne et al. (2022) showed that the presence of low-permeability evaporite units in the Paradox Basin, located on the Colorado Plateau, allowed for the accumulation of He and radiogenic noble gases in underlying confined aguifers. Recent denudation of the Colorado Plateau has also activated deeper meteoric water circulation and partial flushing of basinal brines, as demonstrated by Kim et al. (2022b) through 81Kr dating of groundwaters. However, there has been little consideration of how erosional episodes in the geologic past may have influenced subsurface fluid flow and fluid-rock interactions. By characterizing and dating the rock record of these subsurface flow systems, we can better understand their coevolution and feedbacks with surface processes that are in turn forced by tectonics or climate change. Understanding how the dynamic interplay between climate, surface processes, and subsurface fluid flow systems evolves through time can also provide insights for storage of anthropogenic energy sources and wastes (Birkholzer and Zhou, 2009; Iverson and Person, 2012; von Berlepsch and Haverkamp, 2016; Krevor et al., 2023), mineral and groundwater resource exploration (e.g., Noble et al., 2011), and subsurface microbial life (McIntosh et al., 2023).

High erosion rates in parts of the Colorado Plateau beginning ca. 4 Ma (Murray et al., 2016, 2019) may have deepened the regional topographically driven groundwater flow system or rearranged shallow groundwater circulation patterns if accompanied by the formation of steeper topography. Indeed, Garcia et al. (2018) suggested that precipitation of Fe- and Mn-oxides near faults at 3.6 Ma in the Paradox Basin may reflect these hydrologic changes. The coincidence of rapid erosional exhumation and formation of Fe- and Mn-oxides near the surface at 3–4 Ma motivated us to look for further evidence in the geologic record of reductive fluid flow at this time. Until this study, it has not been clear if widespread bleaching observed across the Colorado Plateau occurred contemporaneously with deep burial, hydrocarbon generation, and upward migration of saline reduced fluids (Kim et al., 2022a), or if reduced fluid flow also occurred at later stages, and if so, what factors may have driven this flow and fluid-rock reaction. It is important to characterize the geochemical characteristics of bleaching to further resolve potential fluid sources and pathways.

In this study, we provide further evidence of synchroneity of red-bed bleaching as well as clay and Mn-oxide mineralization with a distinct Neogene episode of rapid erosional exhumation, and combine the findings with previously published thermochronology and Mn-oxide dating to explore how denudation at the surface may have induced enhanced flow of reduced fluid in the subsurface. We discuss possible mechanistic links between these phenomena. In particular, we consider two scenarios: (1) the formation of steep topography associated with spatially heterogeneous erosional exhumation significantly modified and/or invigorated a regional groundwater flow system that transported fluids, which were reduced from interactions with upgradient hydrocarbon reservoirs, toward shallow discharge zones (Fig. 2) and (2) the drop in pressure and temperature due to erosional exhumation resulted in sudden gas exsolution that created buoyancy and allowed reduced fluids to bleach porous and permeable sandstones (Fig. 2B).

■ BACKGROUND

Geological Background

The Paradox Basin is an ~100,000 km² region on the Colorado Plateau that is defined by the maximum extent of primarily subsurface Late Pennsylvanian evaporite deposits (Fig. 1) near the base of a flexural basin developed in the foreland of the Uncompahgre uplift during the Ancestral Rocky Mountain orogeny (Baars and Stevenson, 1982; Barbeau, 2003). Rapid subsidence adjacent to the Uncompahgre uplift resulted in the deposition of the 2–2.5-km-thick Paradox Formation comprising repeated cycles of organic rich shales, limestones, and evaporites in the Pennsylvanian (Hite et al., 1984; Nuccio and Condon, 1996; Rasmussen and Rasmussen, 2009). Subsequently, coarse-grained detritus of the Permian Cutler Formation shed from the Uncompahgre uplift initiated passive salt-wall growth of the underlying evaporites, which continued through the mid-Mesozoic (Trudgill, 2011). The salt deformation created a series of northwest-southeast-striking fault zones and salt anticlines that separated the basin into hydrologically distinct sub-basins (Trudgill, 2011).

Triassic to Jurassic clastic sedimentary sequences, ranging from 20 to 400 m thick, comprising fluvio-lacustrine, eolian, and sabkha deposits (Moenkopi and Chinle Formations, Wingate Sandstone, Kayenta Formation, Navajo and Entrada Sandstones, and Curtis Formation) with intermittent volcanic ash input, blanket the Paradox Basin with thinner deposits on the flanks of salt anticlines (Nuccio and Condon, 1996). Renewed sedimentation in the Cretaceous led to rapid regional burial and deposition of as much as 2 km of sandstones, coals, and shales such as the Mancos Shale. This phase of relatively rapid burial has been associated with a major phase of hydrocarbon generation in the organic-rich shales of the Paradox Formation (Nuccio and Condon, 1996).

From the Late Cretaceous to early Paleogene, the Laramide orogeny gave rise to the basement-cored, monoclinal uplifts that bound the Paradox Basin, such as the Monument uplift, San Rafael Swell, and Circle Cliffs (Bump and Davis, 2003). Salt movement associated with the Laramide orogeny reactivated faults such as the Moab fault in the latest Cretaceous or Paleocene (Solum et al., 2005; Bailey et al., 2022b). Emplacement of laccolith intrusions occurred ca. 28 Ma, forming the topographically high La Sal, Abajo, and Henry Mountains, which are modern major recharge centers for fresh water (Fig. 1; Hunt, 1956; Nelson et al., 1992; Murray et al., 2016; Barton et al., 2018b). Other important recharge centers include basement-cored uplifts, such as the Uncompangre uplift, and erosional escarpments, such as the Book Cliffs.

Sandstone Bleaching and Paleofluid Flow

The Paradox Basin hosts extensive regions of chemically altered ("bleached") sandstones within the terrestrial Permian to Cretaceous red-bed deposits that were reddened during early diagenesis (e.g., Walker, 1967). The yellow to white bleached sandstones reflect regionally extensive interaction between

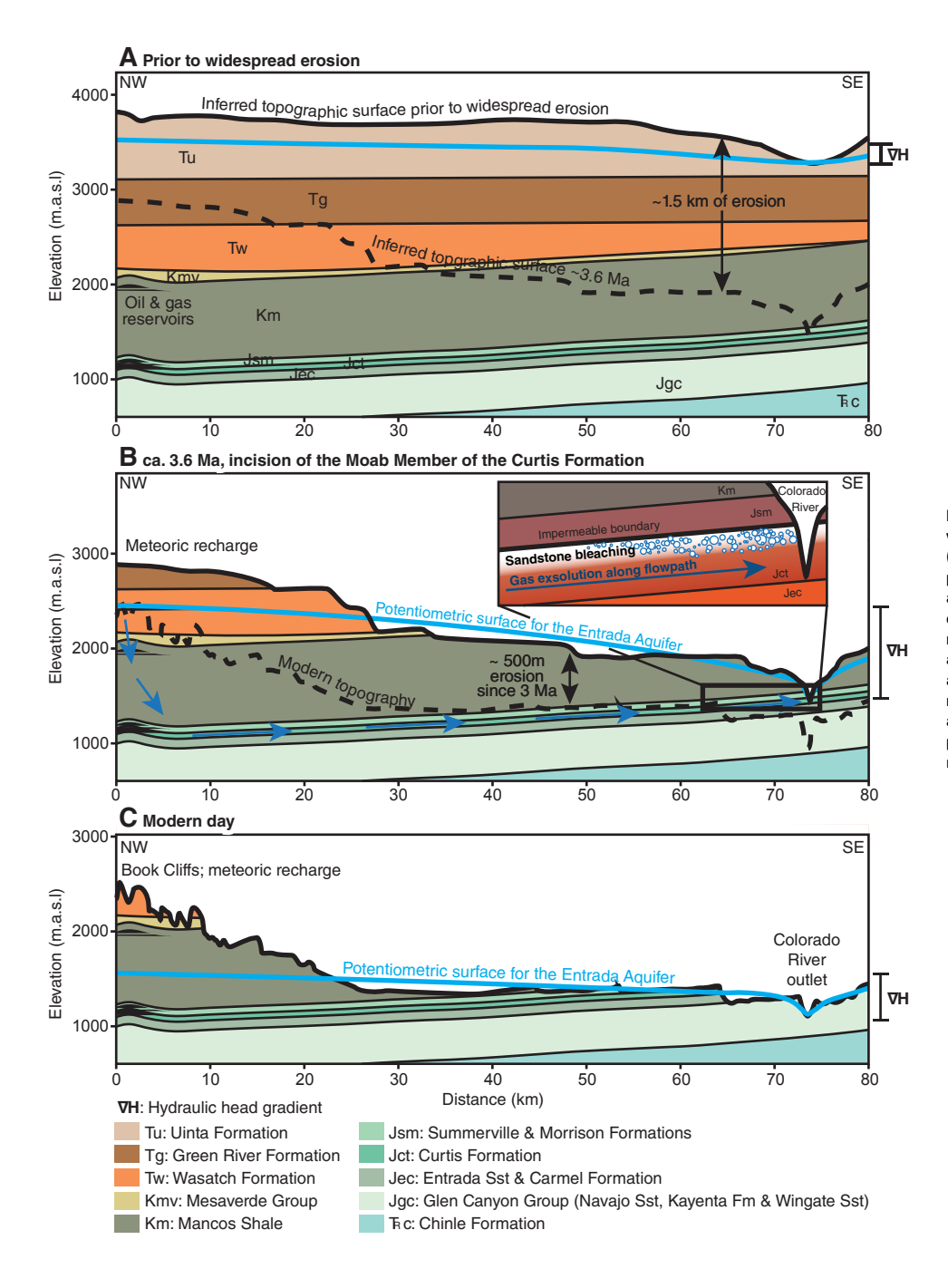


Figure 2. Schematic cross section of the study area prior to widespread erosion (A), at ca. 3.6 Ma (B), and at modern day (C), if erosional exhumation resulted in high-relief topography. Cross sections do not account for regional tilting. Oil and gas reservoirs are present in Cretaceous to Jurassic reservoir rocks. There was ~1.5 km of erosion between A and B, resulting in higher hydraulic gradient. Fluids were recharged at higher elevations, interacted with oil and gas reservoirs, and transported toward discharge zopnes such as the Colorado River. Gases were exsolved from reducing groundwater along the flow path. C shows modern-day topography and potentiometric surface of the Entrada aquifer. m.a.s.l.—meters above sea level; Sst—sandstone; Fm—formation.

the previously red sandstones and fluids containing reducing agents such as hydrocarbons, CH₄, CO₂, and H₂S (Chan et al., 2000; Garden et al., 2001; Beitler et al., 2003; Parry et al., 2004; Kettler et al., 2011; Wigley et al., 2012; Gorenc and Chan, 2015; Bailey et al., 2022a; MacIntyre et al., 2023). The reduced fluids dissolved the Fe-oxide grain coatings that give the sandstones a red pigment. Bitumen is documented only in few study areas (Chan et al., 2000; Eichhubl et al., 2009; Gorenc and Chan, 2015; Bailey et al., 2022a), and otherwise, there is no direct evidence favoring petroleum versus fluids containing dissolved or gaseous CH₄, CO₂, or H₂S as bleaching agents. Loope et al. (2010) used the presence of modern-day CO2 and CH4 fields and lack of bitumen to suggest bleaching of the Navajo Sandstone in the Escalante anticline was the result of CO₂- and CH₂-charged groundwaters. Similarly, Wigley et al. (2012) attributed bleaching of the Jurassic Entrada Sandstone near Green River to CO₂-charged brines containing minor CH₄ based on fluid-inclusion petrography, isotopic data, and geochemical modeling. Geochemical analysis of modern fluids in the Paradox Basin shows that brines sourced from the Pennsylvanian Honaker Trail and Paradox Formations were likely a major source of the reduced fluids responsible for sandstone bleaching (Kim et al., 2022a). Migration of buoyant reducing fluids can explain the bleaching of the Curtis Formation at the crest of the Moab anticline (Garden et al., 2001).

Widespread, laterally extensive bleached sandstones are commonly interpreted as evidence that reduced fluids have caused large-scale ferric Fe dissolution and possible removal, transport, and/or redistribution of iron. Bailey et al. (2022a) suggested that other metals and trace elements such as Mn, Mg, Zn, Pb, and Ti are also remobilized during the flow of reduced fluids. Reduced fluids that transported Fe (and Mn) mobilized during bleaching were a likely source for Fe found in abundant Fe-oxide concretions and larger Fe- and Mn-oxide deposits such as those found at Flat Iron Mesa (Chan et al., 2001, 2007; Beitler et al., 2005; Kettler et al., 2011; Garcia et al., 2018). In some locations, the iron is redistributed and reprecipitated locally over scales of 1–100 cm (Loope et al., 2012; Barton et al., 2018a; Yoshida et al., 2018; Bailey et al., 2022a). In other cases, extensive accumulations of Fe- and Mn-oxide that may have migrated over larger distances appear to be precipitated near redox reaction fronts (e.g., Garcia et al., 2018).

According to Nuccio and Condon (1996), two phases of hydrocarbon generation and expulsion occurred during the Early to Late Cretaceous. Garden et al. (2001) implied, based on unpublished paleomagnetic results, that bleaching took place in the Moab anticline at 49–63 Ma. Migration of petroleum and bleaching of a section of the Entrada Sandstone occurred ca. 41 Ma, based on age determinations on authigenic clay, which coincides with authigenic clay and copper sulfide formation along fault zones (41–48 Ma; Bailey et al., 2022b). It is not clear if all the widespread bleaching observed across the Colorado Plateau occurred contemporaneously with rapid burial, hydrocarbon generation, and migration, or if there have also been more recent phases of reductive fluid flow and bleaching. ⁴⁰Ar/³⁹Ar and (U-Th)/He dating of Fe- and Mn-oxide fracture fill material along fault zones in the Navajo Sandstone indicate formation at 3.6 Ma (Garcia et al., 2018), suggesting flow of reduced fluids

at this time. However, until this study, this 3.6 Ma age had not yet been linked to a phase of red-bed bleaching.

Recent Erosion of the Paradox Basin

Dating constraints on young fluvial deposits suggest integration of separate river drainage networks across the Basin and Range transition zone occurred by 5.6 Ma, and the Colorado River reached the Gulf of California by ca. 4.8 Ma (Lucchitta, 1972; Robert et al., 2010; Crow et al., 2021). This integration of the drainage system and effective regional drop in base level has been proposed to be responsible for kilometer-scale erosion and incision of the Colorado River headwaters, whereby all segments of the river were widened and deepened during transient river incision over the last ~4 m.y. (Hoffman et al., 2010; Karlstrom et al., 2014; Murray et al., 2019). Hoffman et al. (2010) attributed this recent erosion to intensification of the southwest monsoon climate associated with opening of the Gulf of California. River integration and evolving regional groundwater paths on the Colorado Plateau facilitated groundwater sapping, increased groundwater input to younger sedimentary basins downstream of the Paradox Basin, and helped focus erosion (Crossey et al., 2015).

Murray et al. (2016, 2019) used apatite (U-Th)/He thermochronology on rocks in the thermal aureole of the Oligocene laccolith intrusions to resolve the timing and rate of Neogene exhumation in this part of the Colorado Plateau. Thermal modeling of apatite (U-Th)/He dates near the Henry, Abajo, and La Sal Mountains suggest relatively little erosion in the Miocene but as much as ~2 km of erosional exhumation in the past 4 m.y. (Hoffman et al., 2010; Murray et al., 2016, 2019). Murray et al. (2019) suggested that throughout this region, time-averaged erosion rates (averaged to present day) due to regional baselevel lowering were at least 700 m/m.y. (Murray et al., 2016). However, the rate and spatial distribution of erosional exhumation and formation of relief in this region were likely not uniform. Focusing on the Flat Iron Mesa region near Moab, Utah, USA, Garcia et al. (2018) used 4He/3He and (U-Th)/He thermochronology as well as 40Ar/39Ar geochronology on Mn- and Fe-oxides from fault zones near the Canyonlands area to show that the oxides precipitated near the surface ca. 3.6 Ma and have experienced very little erosional exhumation (likely much less than 0.5 km) since then. This variability is consistent with variable incision rates across different regions of the Colorado Plateau since the Late Pleistocene, ranging from <92 m/m.y. near the western Grand Canyon (Arizona, USA; Pederson et al., 2002a) to 350-540 m/m.y. near the Henry Mountains (Cook et al., 2009) to ~900 m/m.y. at Dewey Bridge (Utah) located in the NE part of the Colorado Plateau (Jochems and Pederson, 2015). Thermal modeling combined with the reconstructed post-Laramide topography of the Colorado Plateau shows the greatest amount of Neogene erosion in the Canyonlands region in the north-central plateau near our study area (Pederson et al., 2002b; Hoffman et al., 2010; Lazear et al., 2013). The continued erosion and rock uplift have resulted in a present-day high-relief landscape that might be modulated by knickpoint migration and variable rock strength (Cook et al., 2009; Darling et al., 2012; Bursztyn et al., 2015) as well as feedbacks between erosion, isostatic rebound, and upper mantle dynamics (Karlstrom et al., 2012; Lazear et al., 2013; Pederson et al., 2013).

Topographically Driven Regional Groundwater Flow Systems

In short, parts of the Colorado Plateau, particularly the Canyonlands area and north-central part of the Paradox Basin, experienced as much as 2 km of rapid erosional exhumation between ca. 4 Ma and 3 Ma. This likely resulted in removal of as much as 1000 m of relatively impermeable Cretaceous shale units in at least some places (Figs. 1 and 2B). Resulting changes in hydrostratigraphic architecture (i.e., permeability distribution) may have altered the depth and pattern of meteoric water circulation, especially if erosional exhumation was accompanied by the formation of high-relief topography (Bethke and Marshak, 1990; Ferguson et al., 2018; Kim et al., 2022b). Sufficient potentiometric drive for deep groundwater circulation can be produced by the generation of high-relief topography by denudation or tectonic uplift. For example, basinal brines can be brought close to the surface by denudation (Yager et al., 2017), or the rapid denudation and formation of high relief can enable the deep circulation of meteoric water and flushing of basinal brines (McIntosh and Ferguson, 2021; Kim et al., 2022b). McIntosh and Ferguson (2021) showed that the extent of meteoric water circulation in the crust is strongly controlled by topography and variations in fluid density at depth. Kim et al. (2022b) demonstrated, using 81Kr groundwater age distributions, that there has been deep circulation of meteoric water to as deep as 3 km in the Paradox Basin since at least 1.1 Ma, inferred to have been activated by recent denudation of the Colorado Plateau. This relatively recent deep circulation has dissolved evaporites and partially flushed residual reduced brines from the deep aquifers (Kim et al., 2022a, 2022b). Similarly, significant flushing of deep basinal brines by meteoric water to depths of 6 km has occurred in the northern Uinta Basin, where water recharges along recently (<10 Ma) uplifted basin margins (Zhang et al., 2009).

Removal of shale units and rapid unloading during exhumation may also have resulted in the redistribution of petroleum within the basin, due to either (1) changes in structural configuration or brittle failure of cap rocks or (2) gas expansion or exsolution from oil and formation water (Doré and Jensen, 1996; Doré et al., 2002; English et al., 2016a, 2016b). Topographically driven groundwater flow systems can also mobilize, transport, and even deposit hydrocarbons over long distances (Tóth, 1980; Bethke et al., 1991; Gvirtzman and Stanislavsky, 2000). Immiscible oil slugs have a slower rate of migration but can still be driven laterally across a basin along the tops of regional aquifers (Garven, 1989). Meteoric water recharge has tilted oil-water contacts and flushed and altered oil in reservoirs such as in the San Andres and Grayburg Formations in the Permian Basin, Texas, USA (Hubbert, 1953; Stueber et al., 1998; Saller and Stueber, 2018). In these formations, high elevations created by recent Neogene tectonics increased the hydraulic head to enable meteoric waters to displace dense brines and hydrocarbons (Ramondetta, 1982; Saller

and Stueber, 2018). In the Western Canada Basin, post-Laramide rock uplift triggered a topography-driven hydrodynamic system that allowed long-distance transport and accumulation of the oil preserved in the Mannville Group tar sands (Garven, 1989). Loope et al. (2010) suggested that the Navajo Sandstone to the west of the Paradox Basin, near the Circle Cliffs, was bleached by groundwater that became reduced after topographically driven flow through a CH_4 -charged reservoir.

Therefore, we might expect to find evidence in the rock record for rapid reconfiguration and changes to the subsurface flow system that resulted from erosional exhumation beginning ca. 4 Ma. In this paper, we present the results of characterization and dating of Mn-oxide deposits exposed along the Moab fault as well as of a nearby section of bleached Moab Member of the Curtis Formation to determine how subsurface fluids responded to rapid exhumation. We show that Mn-oxide deposits from this study formed at $3.9 \pm 0.2\,$ Ma, and clay mineralization associated with laterally extensive red-bed bleaching occurred at $3.60 \pm 0.03\,$ Ma. Both of these results, as well as the precipitation of Fe- and Mn-oxides at Flat Iron Mesa at $3.6\,$ Ma (Garcia et al., 2018), are coincident with documented rapid erosional exhumation ca. 3–4 Ma (Murray et al., 2016, 2019; Garcia et al., 2018).

METHODS

Sampling and Whole-Rock Geochemistry

To study the effects of exhumation on the redistribution of reduced fluids in the subsurface, we examined a 50 m section of red (unbleached) and white (bleached) sandstones belonging to the Moab Member of the Curtis Formation (referred to here as the Moab Member sandstone), immediately below shales of the Summerville Formation, near Klondike Bluffs (Fig. 3). We chose this location because of the well-exposed complete section of bleached to red sandstone and the focused bleaching at the top of the sandstone below low-permeability shales (Fig. 4). We collected 13 variably colored sandstone samples of ~1 kg each (7 unbleached, 6 bleached) from above, below, and across the transition from white- to red-colored sandstones (see Supplemental Material¹). The sample spacing distance ranged from 14 m to 50 cm in the red-colored and bleached sandstones to 10 cm in the transition zone. We used X-ray fluorescence (XRF) and inductively coupled plasma mass spectrometry (ICP-MS) to measure the major, minor, and trace element compositions of the samples following the procedures and precision reported in Johnson et al. (1999).

To characterize the manifestation of flow of inferred reductive fluids and presence of redox fronts at the discharge end of a flow system, we also sampled a Mn-oxide deposit exposed along the main segment of the Moab fault

^{&#}x27;Supplemental Material. Includes all calculations and parameters used in this study (mass balance calculations, groundwater transit times, methane required for bleaching, amount of methane exsolved), as well as sample locations. Please visit https://doi.org/10.1130/GEOS.S.25122791 to access the supplemental material, and contact editing@geosociety.org with any questions.

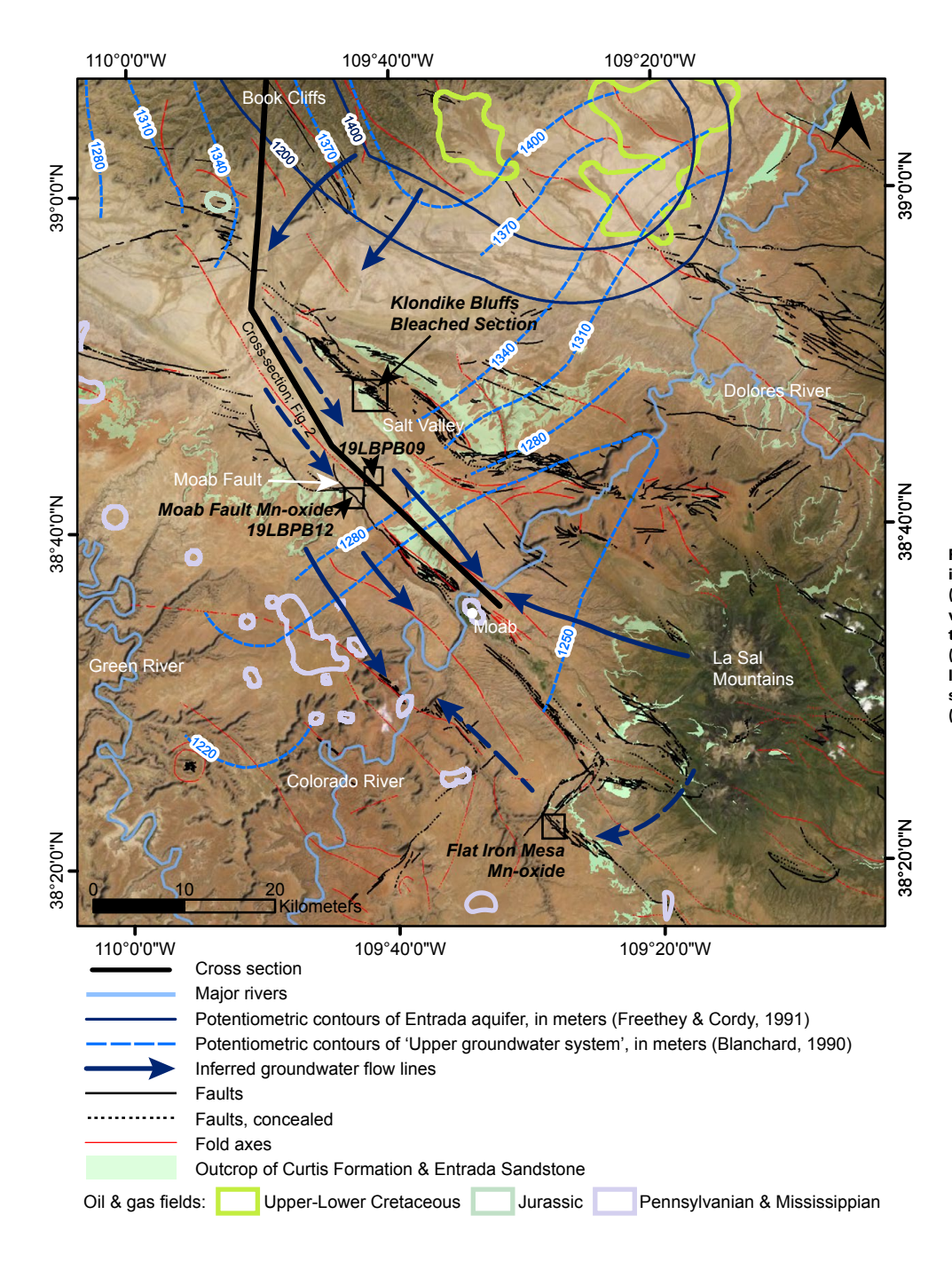


Figure 3. Satellitep-imagery map of the study area showing sample sites (black boxes), major structural features (fault zones—black; fold axes—red), oil and gas reservoirs (green and purple outlines), and regions where the Curtis Formation and Entrada Sandstone crop out (green). Map also shows major river networks (light blue lines), groundwater potentiometric contours (dark blue solid and blue dashed lines), and groundwater flow lines (dark blue arrows).



Figure 4. Outcrop photographs of the studied section of the Moab Member, Curtis Formation. (A) View of entire section. (B) Yellow clay-rich transition zone immediately above the red-bleached boundary. (C and D) Irregular red-bleached boundary cross-cutting stratigraphic features.

(sample 19LBPB12), ~800 m from Courthouse Rock, and a Mn-oxide deposit exposed along the axis of the Courthouse syncline (sample 19LBPB09) (Fig. 3). All sandstone and Mn-oxide samples were imaged using standard optical microscopy and scanning element microscopy (SEM).

Illite Age Analysis

We applied K-Ar dating and illite age analysis to sample 18PRPB52, collected from the studied bleached section of Moab Member sandstone. We chose this sample due to its proximity (within 30 cm) to the bleached-red boundary and high clay concentrations. We applied the same sample preparation, X-ray diffraction (XRD), K, and Ar analysis procedures as outlined in the supplemental material of Bailey et al. (2022b).

We implemented York-type weighted linear regression using the maximum likelihood method (Thirumalai et al., 2011) to correlate the apparent K-Ar ages

on each size fraction to the percent detrital $(2M_1)$ illite (Bailey et al., 2022b) in order to extrapolate the age of the authigenic $(1M_d)$ end-member component. Error on the $1M_d$ authigenic end-member age includes uncertainties from Ar measurements, K measurements, and XRD illite polytype quantification. The code used to perform the linear regression of K-AR ages and illite polytype data is available at https://github.com/lrbgeol/K-Ar-illite.

(U-Th)/He and K-Ar Geochronology of Mn-Oxides

Mn-oxide samples (19LBPB12 and 19LBPB09; Fig. 3) were crushed using a mortar and pestle then cleaned by ultrasonically shaking the samples in ethanol to remove clay and other fine particles from crystal surfaces. We passed the samples through a Frantz isodynamic magnetic separator after drying to separate the oxide cement from matrix minerals such as quartz, feldspar, and calcite. For (U-Th)/He analysis, we identified pure Mn-oxide aliquots using a

Leica MZ16 microscope, packed them into 1 mm Nb foil tubes, and loaded them into a Cu planchet. The planchet was placed in an ultra-high-vacuum gas extraction line, and each aliquot was heated to temperatures of ~850–1000 °C (low to medium glow) for eight minutes using a Nd:YAG laser to extract helium. Aliquots were reheated for ten minutes at a slightly higher lasing intensity to ensure full extraction of ⁴He. The foil packets were then retrieved and transferred to Teflon vials for Parr-bomb dissolution and U-Th-Sm measurements by isotope dilution on a high-resolution Element2 ICP-MS (Reiners, 2005). For Ar isotope analysis, we separated and cleaned the sample as above then sieved to 110–250 µm. We followed the same K and Ar measurement procedures for the Mn-oxides as for the illite.

OBSERVATIONS AND RESULTS

Bleached Moab Member Sandstone at Klondike Bluffs

Mineralogy and Textures

re/article-pdf/doi/10.1130/GES02634.1/6296275/ges02634.p

In our study area near Klondike Bluffs, the upper 6 m of the Moab Member sandstone, immediately below the Summerville Formation, is white to yellow with a sharp boundary between white sandstone and underlying red sandstone

(Figs. 4 and 5). The sharp boundary cross-cuts primary bedding features (Figs. 4C and 4D), and there is no field or petrographic evidence to suggest a difference in primary sedimentary characteristics across it. In general, the Moab Member sandstone is moderately sorted with fine, sub-angular grains.

We used whole-rock major element data to calculate mineral proportions for the sandstone samples by using a least squares method (MINSQ; Herrmann and Berry, 2002). The red sandstone in the lower part of the section has an average normative mineralogy of $75\% \pm 1.3\%$ quartz, $8.3\% \pm 1.8\%$ K-feldspar, $6.2\% \pm 1.3\%$ calcite, $5.9\% \pm 1.3\%$ illite-smectite, $5.4\% \pm 1.9\%$ kaolinite, and $0.60\% \pm 0.10\%$ hematite (Figs. 5 and 6A–6C). The red pigment is formed by thin grain coatings of hematite with illite that surround nearly all detrital grains (Fig. 6C). The calcite cement we observe in the red sandstone is mostly sparite and is irregularly dispersed (Fig. 6a,b). We observe kaolinite mostly as aggregates of kaolinite "booklets" present mostly in the largest pore spaces (Fig. 6B).

Immediately below the sharp transition from yellow to red, the red sand-stone contains slightly higher proportions of clay and calcite, consisting of 70% quartz, 7.2% K-feldspar, 10.8% calcite, 7.5% illite, 4.7% kaolinite, and 0.51% hematite (Figs. 5 and 6D–6F). In contrast to the bulk red sandstone 50 m from the red-yellow boundary, calcite fills most pore spaces, and the porosity of this sandstone is very low (Figs. 6D–6F). Similarly, the yellow sandstone located <30 cm above the boundary also has very low porosity and a high proportion of clay (Figs. 5 and 6l). The yellow sandstone consists of 67.4% quartz, 4.6%

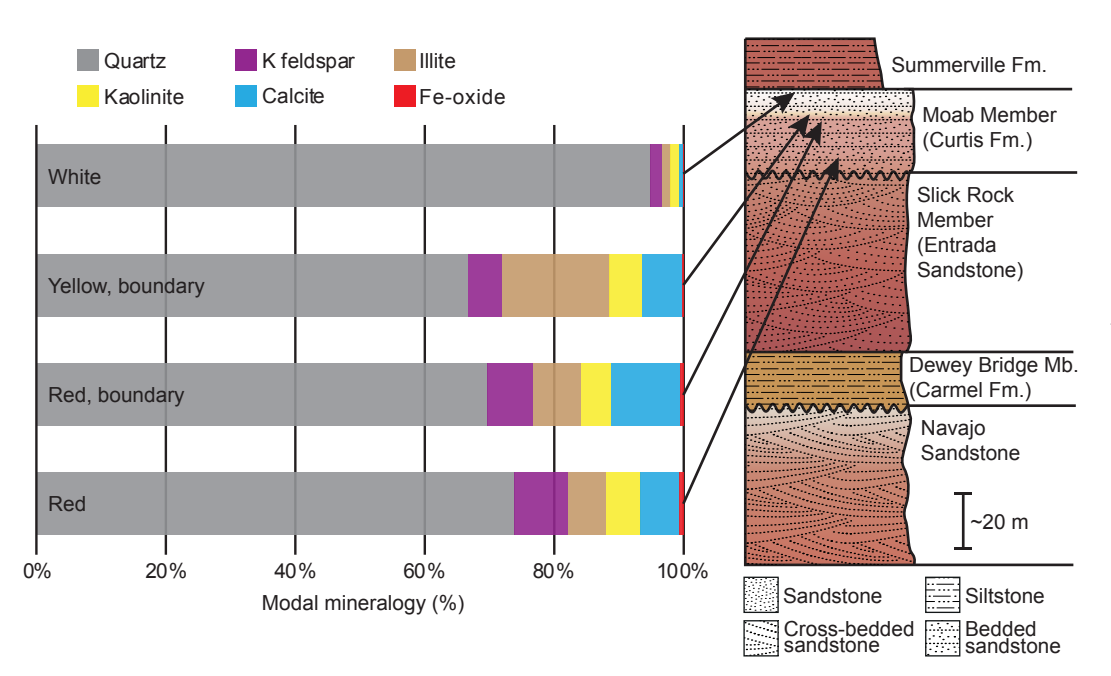


Figure 5. Modal mineralogy of the top white, transition yellow, transition red, and bottom red sandstones calculated from whole-rock geochemistry. Stratigraphic column is adapted from Doelling (2002). Fm.—Formation; Mb.—Member.

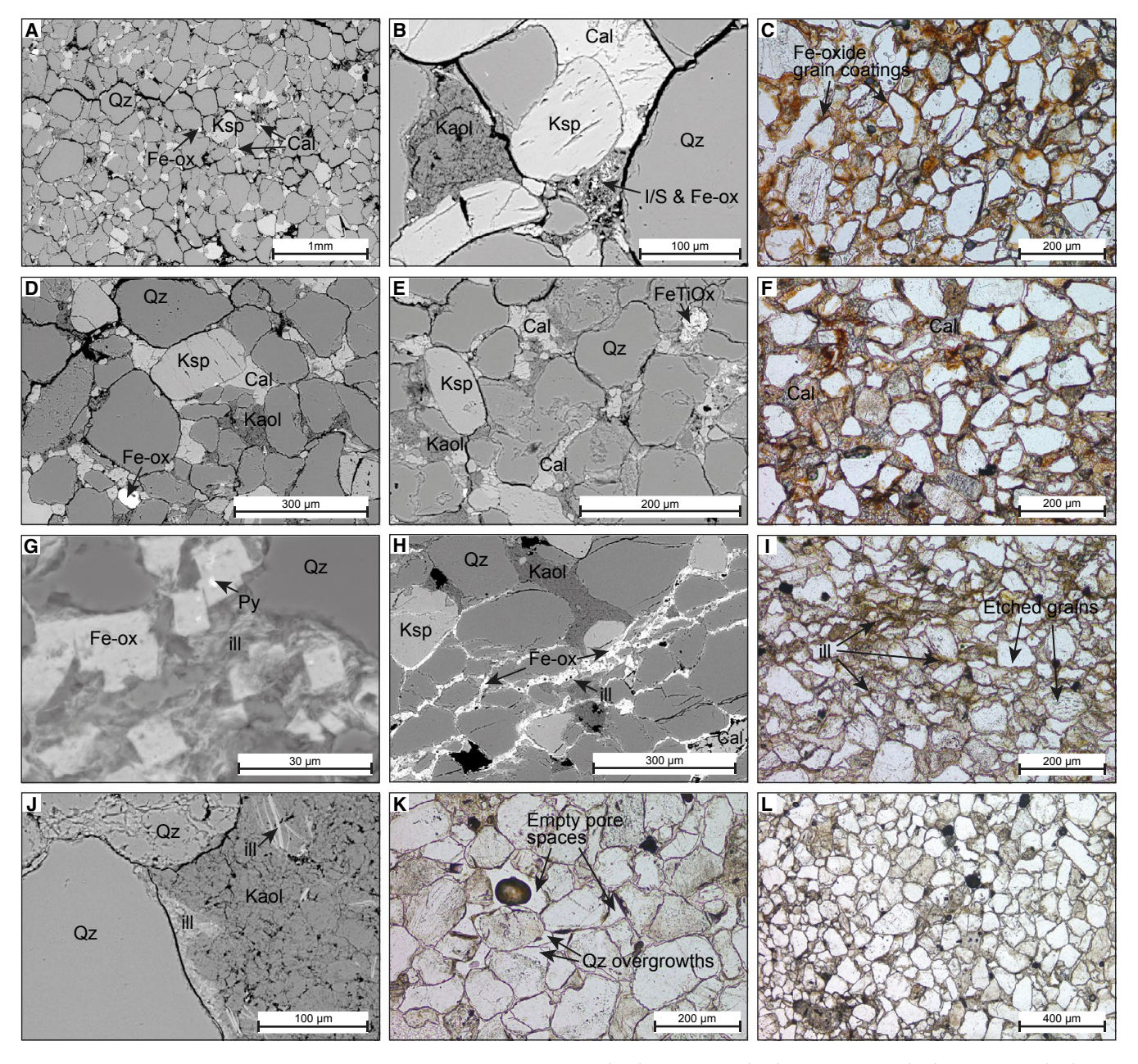


Figure 6. Secondary electron microscope and thin-section photomicrographs of the red (A-C), red-transition (D-F), yellow-transition (G-I), and top white (J-L) Moab Member sandstones from the studied section. Qz - quartz; Ksp - K-feldspar; ox - oxide; Cal - calcite; I/S - illite/smectite; Kaol - kaolinite; Py - pyrite; ill - illite.

K-feldspar, 5.5% calcite, 17% illite, 5.1% kaolinite, and 0.27% Fe-oxide. The illite particles are wispy in texture, fill most pore spaces, and are closely associated with small cubes of Fe-oxide (Fig. 6G). We observe remnant pyrite in the center of some of these Fe-oxide cubes (Fig. 6G). The Fe-oxide cubes are mostly concentrated in "stringers" between detrital grains (Fig. 6H).

The color of the Moab Member sandstone progressively changes from yellow to white toward the top of the section (Figs. 4 and 5). The white sandstone consists of 95% quartz, 1.7% K-feldspar, 0.5% calcite, 1.3% illite, 1.4% kaolinite, and 0.1% Fe-oxide and has the highest porosity in the section (Fig. 6L). We observe euhedral quartz overgrowths (Fig. 6K) and small zones containing pore-filling kaolinite and illite (Fig. 6J).

Whole-Rock Geochemistry

We observe systematic differences in major, minor, and trace elements between the white-tan bleached sandstone and the unbleached red sandstone, as well as large compositional gradients within 1 m of the white-red interface (transition zone) (Figs. 7 and 8).

The red sandstone, on average, has lower SiO₂ concentrations of 88.4% ± 1.56% than the uppermost white sandstone (96.0% ± 1.69%). In contrast, average concentrations of Al₂O₃, CaO, and K₂O are higher in the red sandstone (4.93% ± 0.54%, 3.68% ± 1.5%, and 1.92% ± 0.10%, respectively) compared to the white sandstone (2.41% \pm 1.00%, 0.17% \pm 0.11%, and 1.06% \pm 0.48%, respectively). Similarly, the red sandstone has higher Fe₂O₃, MnO, and MgO $(0.75\% \pm 0.13\%, 0.03\% \pm 0.01\%, \text{ and } 0.21\% \pm 0.03\%, \text{ respectively})$ as well as trace metals such as Cr, V, Cu, and Zn (14.2, 13.5, 6.1, and 6.9 ppm, respectively) than in the white sandstone (Fe₂O₃ $0.24\% \pm 0.10\%$, no MnO, MgO 0.08%± 0.04%, Cr 9.2 ppm, V 7.96 ppm, Cu 7.81 ppm, and Zn 3.47 ppm). In fact, all major and minor metals and rare earth elements (REEs) except for Ni and Cu have higher concentrations in the red sandstone compared to the uppermost white sandstone (Fig. 8). The magnitude of the Eu [Eu/Eu* where Eu* = (Sm × Gd)^{1/2}] anomaly is lower (0.91 versus 0.84) and the magnitude of the Ce [Ce/ Ce* where $Ce^* = (La \times Pr)^{1/2}$ anomaly (using C1 chondrite-normalized concentrations) is indistinguishable (0.91 versus 0.90) in the bleached sandstone relative to the red sandstone. However, the Eu anomaly is most negative and the Ce anomaly least negative just above the interface.

In contrast, the yellow-colored samples taken within 30 cm of the interface between the red and white sandstones have the highest concentrations of most elements, including REEs, compared to both the red- and white-colored sandstones. Notably, Al_2O_3 and K_2O concentrations are 6.31% and 2.29%, respectively, and the sum of REEs is 48 ppm in the yellow sandstone immediately above the bleached-red interface (Figs. 7E–7H and 8E–8H), higher than observed in the red sandstone. Although both the Eu and Ce anomalies vary little across the sampled transect, Eu/Eu* is lowest at 0.81 and Ce/Ce* is highest at 0.93 within 30 cm above and below the interface. In contrast to the other elements that have their highest concentrations within 30 cm of the

interface, SiO_2 (87.4%) concentrations are lowest at the interface compared to the rest of the sampled column. Additionally, the two red sandstone samples immediately below the bleached-red transition have the highest concentrations of CaO (5.44%) and MnO (0.04%) (Figs. 7F–7H).

Overall, the bleached sandstones are depleted in all elements except for SiO_2 , Ni, and Cu when compared to the red sandstones. The most notable variations in concentration with respect to position in the sequence occur within 30 cm of the bleached-red interface. At this interface, we observe the highest Al_2O_3 , K_2O , Fe_2O_3 , MgO, and TiO_2 concentrations as well as trace and REE contents but the lowest SiO_2 and U concentrations. The highest concentrations of CaO and MnO, in contrast, occur ~20 cm below the interface, in the red sandstone.

Clay Mineralogy and K-Ar Dates

We separated clay from the bleached sandstone we collected immediately above the bleached-red interface. This sample had the highest clay content, corresponding also to the highest Al $_2$ O $_3$ and K $_2$ O concentrations. All the separated clay size fractions consisted of $1M_d$ illite, $2M_1$ illite, kaolinite, and smectite in varying proportions (Table 1). Other phases identified in the clay samples include quartz, calcite, K-feldspar, plagioclase, and hematite. The finest size fraction contained no quartz, K-feldspar, or plagioclase but contained the most calcite.

Relative proportions of the illite polytypes are displayed in Table 2. The relative proportion of the $2M_1$ (detrital) illite polytype decreases from 43.4% in the 1–2 μm fraction to 0% in the finest (<0.05 μm) fraction (Fig. 9; Table 2). Conversely, the $1M_d$ (authigenic) illite proportion increases from the coarsest size fraction and makes up 100% of illite in the finest size fraction. This coincides with an increase in K concentrations, from 1.3 wt% in the 1–2 μm fraction to 10.4% in the <0.05 μm fraction, and a decrease in the K-Ar date. The K-Ar dates are 159, 117, 88.0, and 3.61 Ma for the 1–2, 0.2–1, 0.05–0.2, and <0.05 μm fractions, respectively. Due to the finest size fraction containing no detrital illite, we can use the total gas age for this fraction as our $1M_d$ end-member age (3.61 \pm 0.03 Ma). In addition, the $1M_d$ end-member date using weighted linear regression on all the separates yields an indistinguishable age from the total gas age of the finest size fraction date of 3.60 \pm 0.03 Ma (r^2 = 1.0) (Fig. 9).

Mn-Oxides

Mineralogy, Textures, and Paragenetic Sequences

Sample 19LBPB12, collected from the Moab fault (Fig. 3), is a brecciated mass of Mn-oxide and calcite with a botryoidal texture. The Mn-oxide deposit is situated within the fault gouge or damage zone of the Moab fault, with the Navajo Sandstone exposed in the footwall and the Brushy Basin Member of the Morrison Formation exposed in the hanging wall. The fault zone consists

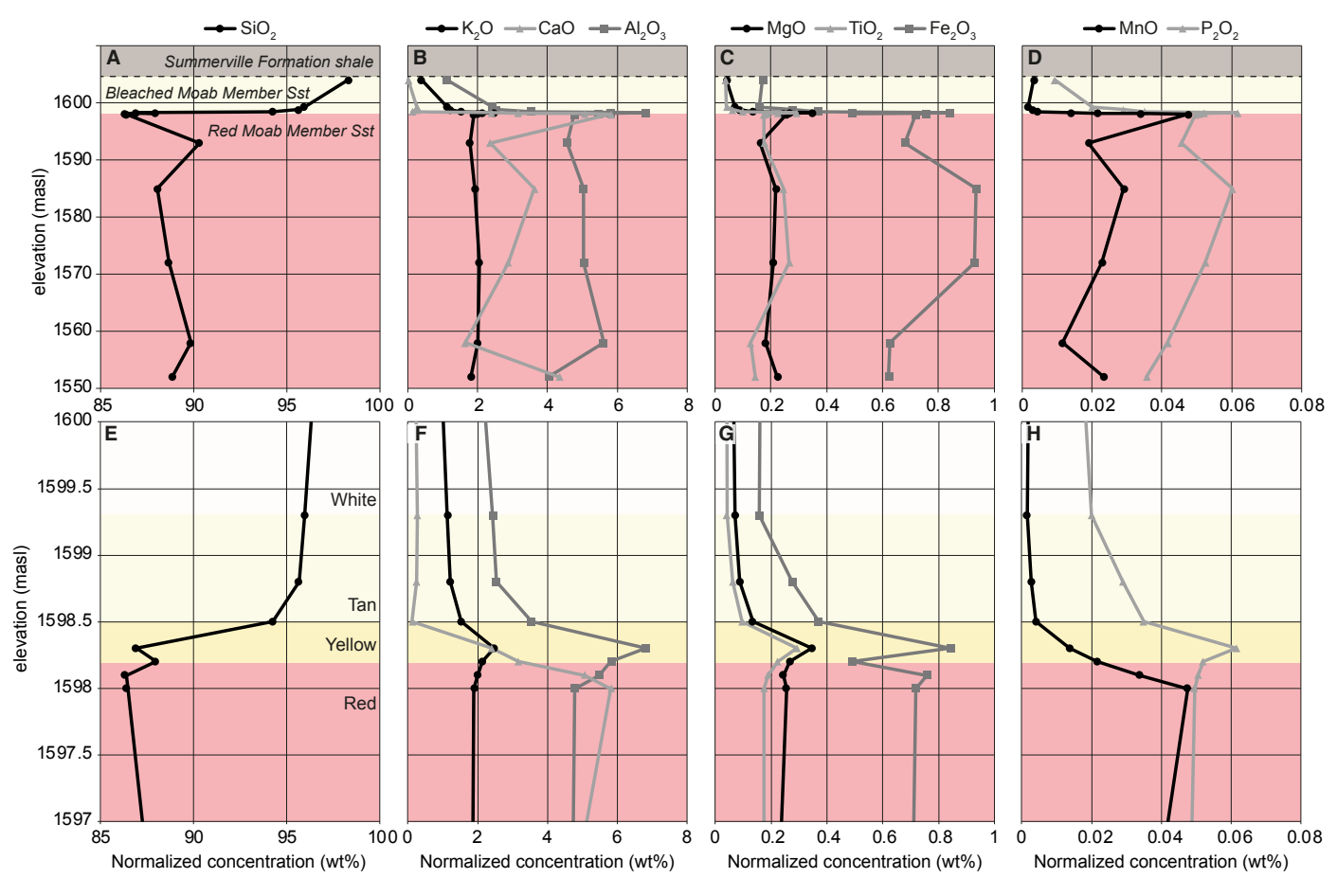


Figure 7. Major (A–C and E–G) and minor (C–D and G–H) element data for the bleached section of the Moab Member, Curtis Formation. Panels E–H are zoomed in versions of panels A–D, respectively, showing the red-bleached transition. Most geochemical changes occur in the yellow zone. masl—meters above sea level; Sst—sandstone.

of clay-rich and weakly consolidated material that has been more susceptible to erosion than the wall rocks.

Colloform bands in the Mn-oxides alternate between calcite, amorphous and/or cryptocrystalline Mn-oxide, and microscale fibrous or more granular Mn-oxide (Figs. 10A and 10B). Calcite is present in the center of many of the colloform bands (Fig. 10B). The fibrous Mn-oxide contains as much as 1% Ba, whereas the amorphous Mn-oxide contains no measurable Ba. Nearly all the observed Mn-oxide contains K (as high as ~3%). Mn-oxide occurs as granular crystals within the matrix or as band-perpendicular fibrous crystals on the outermost bands and has the lowest K concentration (~1%) (Fig. 10A).

The main Mn-oxide mineral present is likely cryptomelane with minor impure hollandite. The maximum size of observable continuous Mn-oxide domains at this microscopic scale (which may be a proxy for maximum crystal size) is ~20 µm. Relatively large Fe-oxide cubes (20–30 µm) are present within the matrix, and fine-grained masses of small, Fe-oxide cubes (<5 µm) occur on the outside edge of some of the Mn-oxide bands (Fig. 10D). In the center of the largest cubes, pyrite can be observed, consistent with Fe-oxide replacement of pyrite (Fig. 10D). Barite is present as large, euhedral plate-like crystals or as late-stage colloform banding (Fig. 10C). Calcite veins, forming the brec-ciated texture, cross-cut the Mn-oxide colloform textures, Fe-oxide, barite,

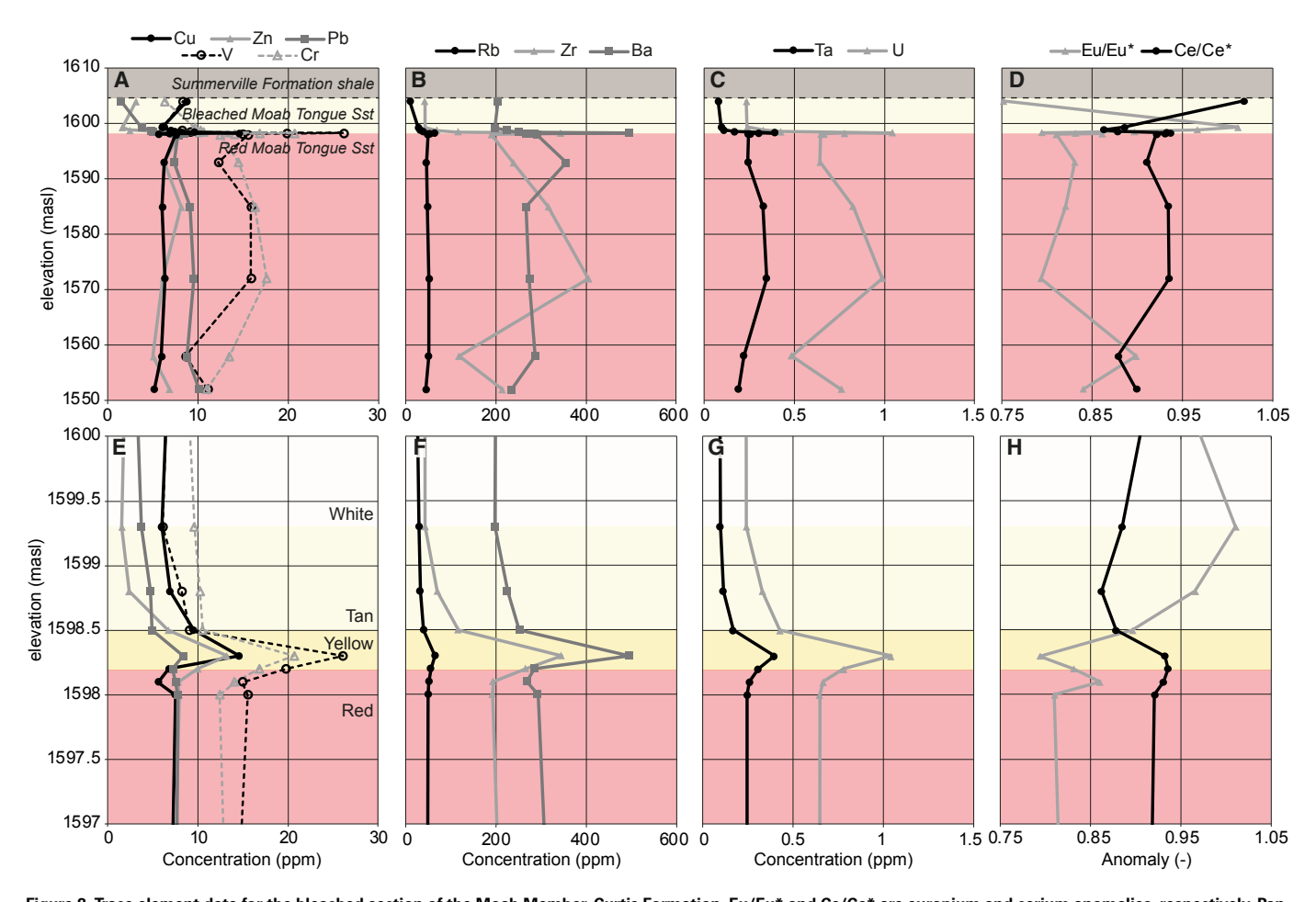


Figure 8. Trace element data for the bleached section of the Moab Member, Curtis Formation. Eu/Eu* and Ce/Ce* are europium and cerium anomalies, respectively. Panels E-H are zoomed in versions of panels A-D, respectively, showing the red-bleached transition. Note the increase in concentrations of nearly all trace elements in the yellow section compared to the red, tan, and white sections. masl—meters above sea level; Sst—sandstone.

and quartz matrix (Fig. 10C). The concentration of Fe in the Mn-oxides is <1%. Overall, there are three main types of Mn-oxide textures in sample 19LBPB12: (1) amorphous and/or cryptocrystalline K-rich (likely cryptomelane) Mn-oxide bands, (2) fibrous to microscale needle-like bands of Ba-containing Mn-oxide (impure hollandite), and (3) granular to in some cases rhombic masses of K-rich Mn-oxide. The first and second type of texture occur as alternating colloform bands, whereas the third texture appears to represent a later stage of crystallization within the matrix. Due to our sampling technique, the fine grain size, and syngenetic nature of the Mn-oxides, all three types of Mn-oxides

observed in sample 19LBPB12 were likely present in the individual aliquots used for K-Ar and (U-Th)/He dating.

The sample location of sample 19LBPB09 is \sim 3 km from that of sample 19LBPB12 and is in the Brushy Basin Member of the Morrison Formation in the hanging wall of the Moab fault. The outcrop is situated near the fold axis of the Courthouse syncline. In outcrop, Mn-oxide occurs as dense, pore-filling cement in round concretions within conglomerate and sandstone lenses. The Mn-oxide cement is compositionally homogeneous and contains no K and is most likely almost pure hollandite. Crystal sizes range from \sim 5 μ m to as large as 40 μ m.

TABLE 1. MINERAL COMPOSITION OF SEPARATED CLAY SIZE FRACTIONS FROM BLEACHED MOAB MEMBER SANDSTONE, DETERMINED BY X-RAY DIFFRACTION

Size fraction (µm)	1M _d illite (%)	2M ₁ illite (%)	Kaolinite (%)	Smectite (%)	Quartz (%)	K-feldspar (%)	Plagioclase (%)	Calcite (%)	Mg-calcite (%)	Chlorite (%)	Hematite (%)	Rutile (%)
1.0-2.0	4.9	3.8	68.6	11.1	3.9	0.0	0.0	7.7	0.0	0.0	0.0	0.0
0.2-1.0	4.4	1.9	64.2	21.5	1.5	1.7	0.4	4.1	0.0	0.0	0.3	0.0
0.05-0.2	28.9	7.9	19.7	29.2	0.1	1.0	5.9	2.8	0.0	4.2	0.4	0.0
< 0.05	4.1	0.0	8.8	27.3	0.0	0.0	5.5	43.1	7.8	0.0	0.0	3.4

Notes: 1M_d illite—authigenic; 2M₁ illite—detrital

TABLE 2. PROPORTION OF ILLITE POLYTYPES, POTASSIUM CONCENTRATION, K-Ar AGE, AND END-MEMBER AGES OF CLAY SEPARATED FROM BLEACHED MOAB MEMBER SANDSTONE

Size fraction (µm)	1M _d illite (%)	2M ₁ illite (%)	K (%)	Total gas age (Ma)	Uncertainty (1σ)	100% 1M _d age (Ma)	Uncertainty (1σ)	100% 2M₁ age (Ma)	Uncertainty (1σ)	
1.0-2.0	56.6	43.4	1.3	159.2	2.0		0.03	344.5	17.5	
0.2-1.0	69.4	30.6	2.5	116.6	1.0	3.6				
0.05-0.2	78.6	21.4	3.3	88.0	0.9	3.0				
<0.05	100.0	0.0	10.4	3.6	0.0					
Notes: 1M _d illite—authigenic; 2M ₁ illite—detrital.										

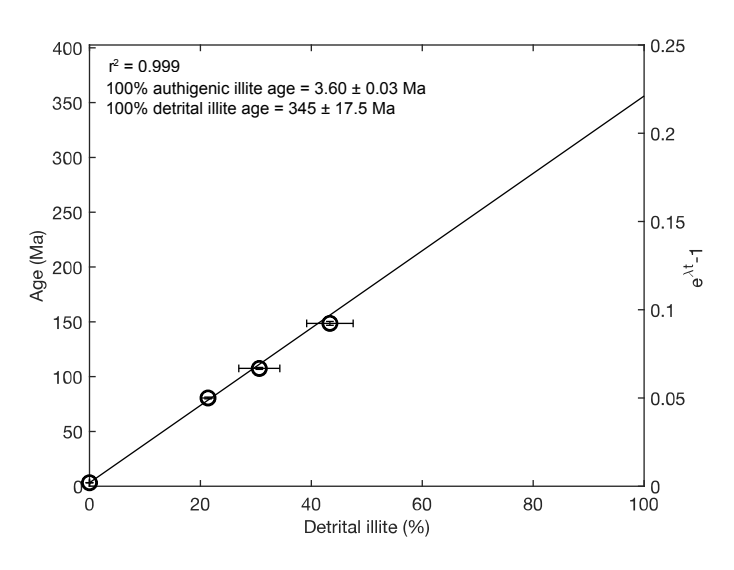


Figure 9. Illite age analysis plot showing the age (Ma) and detrital illite (%) of clay size separates from the bleached sandstone. Detrital illite is linearly related to the decay constant of potassium, λ (= 5.543 × 10⁻¹⁰), so is plotted against e^{λ} –1 (t = age in years). Note that the youngest and finest size fraction is 100% authigenic illite, producing an end-member authigenic illite age of 3.60 ± 0.03 Ma. Error bars are 1c.

K-Ar and (U-Th)/He Dates

The Mn-oxide samples taken from the Moab fault (19LBPB12) and adjacent to the fault in the Courthouse syncline (19LBPB09) have (U-Th)/He ages ranging from 0.12 \pm 0.03 to 3.10 \pm 0.09 Ma and 0.17 \pm 0.05 to 2.63 \pm 0.08 Ma, respectively (Fig. 11). We omitted samples from further consideration if they had >15% (1 σ) analytical uncertainty, primarily due to very low He contents. Only sample 19LBPB12 contained sufficient K (1.45%) for K-Ar dating, and it yielded an average age of 3.9 \pm 0.2 Ma (calculated from three aliquots), which is older than the (U-Th)/He ages for both samples.

DISCUSSION

Bleaching of the Moab Member Sandstone

We interpret the color and geochemical variations in the studied section of the Moab Member sandstone to be the result of reaction with reducing fluids. The sharp boundary between the unbleached and bleached sandstone is undulating and cross-cuts primary sedimentary features such as lamination and stratigraphic bedding (Figs. 4C and 4D). We also observe no significant difference in the average grain size or sorting across this boundary that might represent a change in depositional environment. Based on comparing the lowest

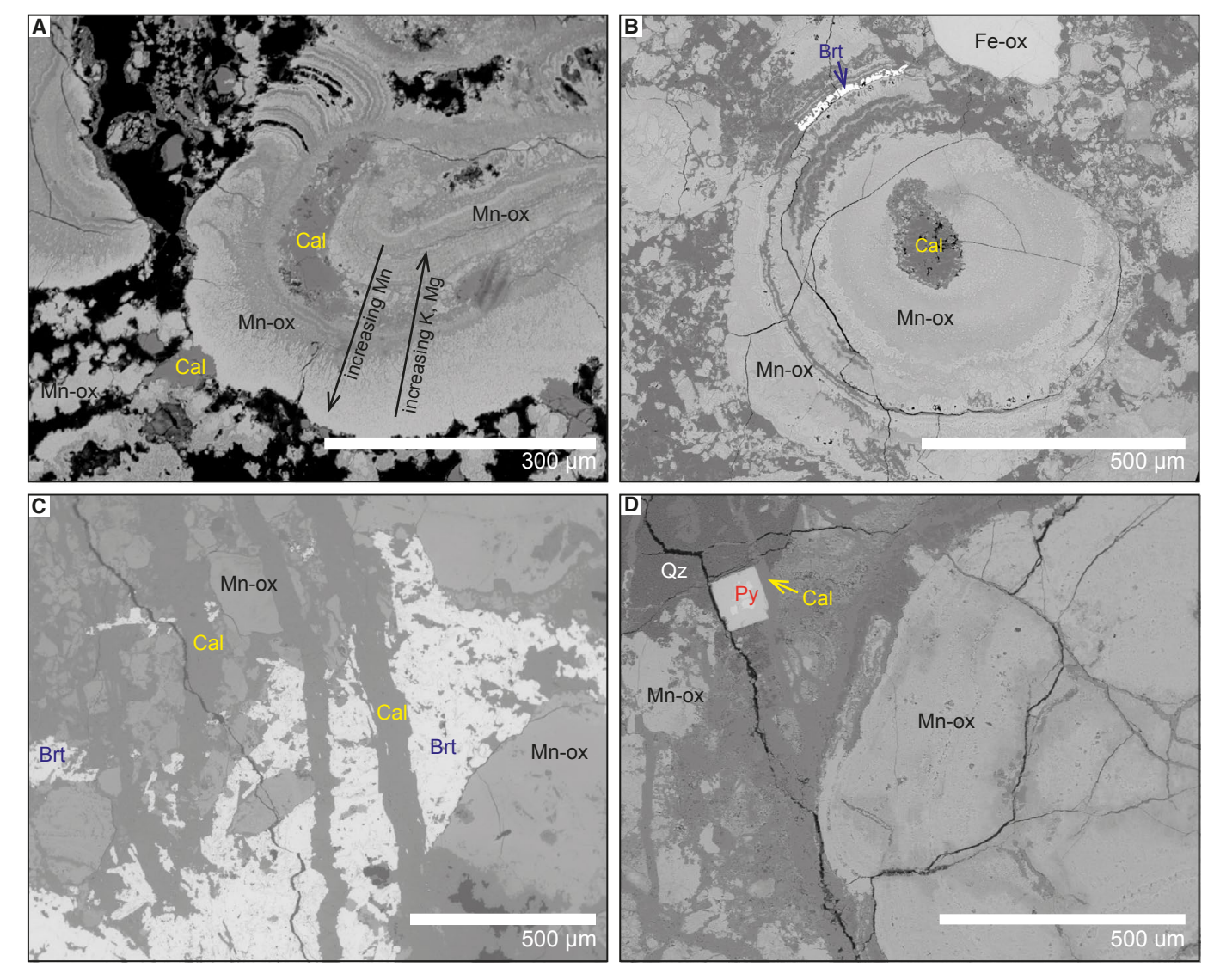


Figure 10. Secondary electron microscope images showing textures and composition of sample 19LBPB12. (A) Colloform and botryoidal textures of alternating Mnoxide (Mn-ox) and calcite (Cal). (B) Colloform and botryoidal textures showing a calcite core and some barite (Brt) layers. (C) Mn-oxide and barite cross-cut by late-stage calcite veins. (D) Colloform Mn-oxide and pyrite (Py) cubes. Qz—quartz.

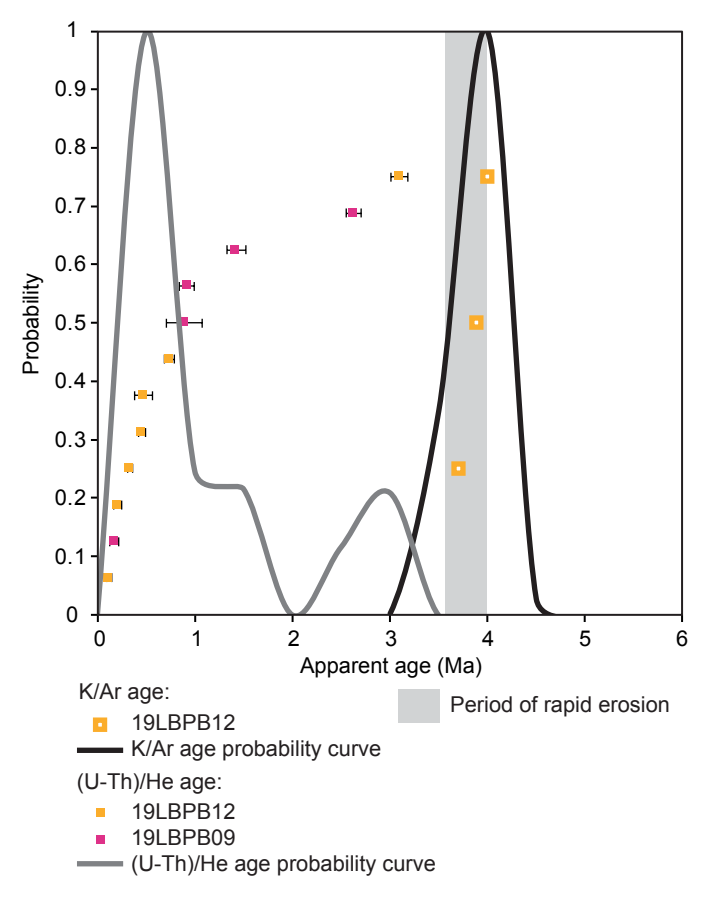


Figure 11. Relative probability plot of K-Ar and (U-Th)/He ages of Mn-oxide samples, with key event as gray bar. All (U-Th)/He ages are younger than K-Ar ages. Error bars are 2σ.

red sandstone with the uppermost white sandstone (Figs. 6C and 6L), the color difference is likely a result of the presence or absence of Fe-oxide grain coatings. Geochemical analysis of the unbleached and bleached sandstones reveals not only a decrease in Fe₂O₃ concentrations in the bleached sandstones but lower concentrations in all elements except for SiO₂. This suggests significant mobilization of all elements, including high-field-strength elements that are typically considered relatively insoluble and immobile. Similar compositional differences were also observed in other studies of bleached Entrada, (Wigley et al., 2012; Bailey et al., 2022a), Wingate (Thorson and MacIntyre, 2005; MacIntyre et al., 2023), Navajo (Beitler et al., 2003, 2005), and White Rim Sandstones (Gorenc and Chan, 2015). Under reducing conditions, Ce is released into the fluid from

Fe-oxide grain coatings, and therefore, the altered sediments would show a more pronounced negative anomaly compared to Fe-oxide-rich oxygenated sediment, which have less-negative to sometimes positive Ce anomalies (Wilde et al., 1996). Reduction of Eu occurs only in highly reducing conditions and most commonly in high-temperature environments. Less-negative or sometimes positive Eu anomalies can occur if authigenic minerals such as illite in the altered sandstone precipitated from fluids that dissolved Eu-rich phases such as plagioclase (Uysal and Golding, 2003; Ziegler et al., 2007).

The yellow, clay-rich sandstone immediately above the bleached-red interface, in contrast to the uppermost bleached white sandstone, has the highest concentrations of all elements except for Si, and Ca and Mn, which are concentrated immediately below the red-bleached boundary. One potential explanation for the higher concentrations of many elements in the clay-rich transition zone is that they were mobilized from the overlying highly bleached white sandstone and transported to the low-permeability transition zone above the unaltered red sandstone beneath. To address this hypothesis, we conducted a simple mass balance calculation. We organized the data according to four main zones in the sampled section: (1) red sandstone, interpreted as the "protolith;" (2) red calcite-rich sandstone immediately below the red-bleached transition; (3) yellow, clay-rich sandstone immediately above the red-bleached transition; and (4) the uppermost white sandstone at the top of the bleached section below the Summerville Formation. Assuming the thickness of each zone we measured at the study site is laterally continuous, we then calculated the relative proportion of major, minor, and trace elements in each zone. We assumed that the bleached sandstone had the same geochemical composition as the red sandstone prior to flow of reducing fluids. We found that only ~30% of the Fe₂O₂, TiO₂, and Zr and ~15% of MnO and CaO observed in the red sandstone are accounted for in the clay-rich transition zone. About 45%-57% of Al₂O₃, K₂O, and MgO are accounted for in the clay-rich zone, most of which is likely hosted in the high concentrations of authigenic illite. Similarly, the clay-rich zone accommodates between 30% and 55% of nearly all trace metals and REEs that have been removed from the white sandstone. The most notable exceptions are Ni and Cu, which have much higher overall concentrations in the white and clay-rich sandstone than in the protolith red sandstone, suggesting an external source of these metals.

These calculations show that if the bleached white sandstone had an initial composition of the lower red sandstone and reducing fluids dissolved and mobilized most elements within it, then only about half of most elements were redeposited locally in the clay-rich layer above the sharp boundary. This means that significant concentrations of all elements except Si may have been transported longer distances, presumably laterally, away from the studied area, given that there is missing mass.

Copper and Ni, interestingly, have much higher concentrations in the clay-rich zone than can be accounted for just by remobilization from the red sandstone. Both Cu and Ni are mobilized in oxygenated conditions (Rinklebe and Shaheen, 2017). We suggest that these metals were possibly enriched in the clay-rich zone by a later stage of oxidized fluid flow, where Cu and Ni were geochemically trapped by the presence of sulfides (pyrite) associated with the clays, consistent

with interpretations in other Cu accumulations in the Paradox Basin such as at Lisbon Valley (Hahn and Thorson, 2005), in the Wingate Sandstone (Thorson, 2004, 2018; Thorson and MacIntyre, 2005; Barton et al., 2018a; MacIntyre et al., 2023), and in the paleo-oil reservoir in the Slick Rock Member of the Entrada Sandstone ("Rainbow Rocks;" Bailey et al., 2022a). Lack of organic material such as bitumen in this section may have prevented other metals such as U and V from being similarly enriched by late-stage oxidized fluids, as in Rainbow Rocks (Cumberland et al., 2016; Barton et al., 2018b; Thorson, 2018).

Timing of Mn-Oxide Formation and Sandstone Bleaching

Mn-oxide (U-Th)/He ages from this study range from 0.12 to 3.1 Ma, all younger than the Mn-oxide K-Ar age of 3.9 ± 0.2 Ma (Fig. 11). This age distribution for He and Ar chronometers is very similar to that of the Mn-oxides reported by Garcia et al. (2018) in that the oldest (U-Th)/He Mn-oxide ages approach the K-Ar (or 40Ar/39Ar) age. Garcia et al. (2018) used helium fractional retention models, ⁴He/³He step-heating diffusion experiments, and ⁴⁰Ar/³⁹Ar plateau ages to show that the Fe- and Mn-oxide deposits at Flat Iron Mesa formed at 3.6 Ma close to modern surface temperatures, consistent with very little erosional exhumation at that locality since 3.6 Ma. The observed variability in the (U-Th)/He ages, which are generally younger than the 40Ar/39Ar ages of the same samples, was interpreted to be a result of diffusive He loss (Reiners et al., 2014; Garcia et al., 2018). Calculated He closure temperatures for Mn-oxides were only ~17 °C (Garcia et al., 2018), so it is likely that samples from our study also experienced variable radiogenic He loss, yielding a similar distribution of ages that approach a maximum represented by the K-Ar age. In contrast, radiogenic Ar is released from cryptomelane only at temperatures >~300 °C (Vasconcelos et al., 1995), and therefore, we interpret our K-Ar age of 3.9 Ma of the Moab fault sample to represent the Mn-oxide formation age and the younger (U-Th)/He ages to represent variable radiogenic He loss.

We show that the interstitial clay in the bleached Moab Member sandstone is primarily detrital illite, authigenic illite, kaolinite, and smectite occurring as pore linings and fillings. The authigenic clay minerals are intergrown and closely associated with (now oxidized) pyrite cubes, suggesting they formed during the flow of reduced fluids containing sulfur (Fig. 6G). The $1\,\mathrm{M}_\mathrm{d}$ endmember age from illite age analysis and the date of the finest size fraction suggests that the authigenic clay formed at $3.60 \pm 0.03\,\mathrm{Ma}$.

Erosional History

Thermal modeling of apatite low-temperature thermochronology results near the Henry Mountains show that ~80% of good-fit time-temperature (t-T) paths cooled below 40 °C only after 4 Ma (Murray et al., 2016). Apatite age-effective uranium (eU) and t-T histories from the La Sal and Abajo laccolith centers, the Colorado River–Green River confluence, and Lees Ferry (Arizona)

in the Paradox Basin are very similar to those of the Henry Mountains and require a rapid pulse of cooling sometime after 6 Ma (Murray et al., 2019).

Murray et al. (2016) suggested time-averaged exhumation rates from 5 Ma to present day of ~0.2–0.7 km/m.y. If we assume that 1.5 km of erosion in the study area occurred only between 4 and 3.6 Ma—based only on the amount of cooling observed in apatite thermal histories of Murray et al. (2016, 2019) and Mn-oxide helium fractional retention models of Garcia et al. (2018)—then time-averaged exhumation rates may have been as high as 3750 m/m.y. Fleming (1994) used the stratigraphic distribution of reworked Cretaceous pollen to suggest the headwaters of the Colorado River reached and began to erode the Mancos Shale in southeastern Utah ca. 3.9 Ma. Using predicted pre-erosional thicknesses of the Mancos Shale in the study area (1144–1250 m; Doelling, 2002) and erosion rates of 3750 m/m.y., the Mancos Shale would have been fully eroded and breached by 3.60–3.57 Ma.

Local erosion rates this high could have been accommodated by high rates of lateral escarpment retreat (e.g., the Book Cliffs; McCarroll, 2019) or knickpoint propagation. Localized high erosion rates in the Paradox Basin can also be attributed to salt dissolution (Guerrero et al., 2015; Mauch, 2018). Although erosion rates integrated over broad areas would be lower than this, local rates can be rapid over short durations, especially in a high-relief landscape consisting of rocks of different erodibilities like in the Paradox Basin. For example, cosmogenic ¹⁰Be concentrations from samples in Grand Staircase-Escalante National Monument show large variability in erosion rates ranging from 20 to >3500 m/m.y., which have been attributed to lithologically controlled escarpment retreat and a landscape adjusting to base-level fall (Riley et al., 2019). However, the authors of the study noted that rates calculated from ¹⁰Be values within a transient landscape may not be accurate (Riley et al., 2019). Therefore, given that our calculated erosion rates are based on the limited available thermochronologic data and do not account for spatial variation, these rates may just represent maximum values but nevertheless signify a period of rapid erosion.

The coincidence of the red-bed bleaching, Mn-oxide precipitation, and timing of rapid erosional exhumation is intriguing, and in the following discussion we address how denudation at the surface is a mechanism that could have induced a phase of reduced fluid flow in the subsurface. We discuss two hypotheses (not mutually exclusive) by which such a connection might have operated: (1) The formation of steep topography associated with erosional exhumation activated a regional groundwater flow system, whereby deep meteoric water circulation flushed reduced fluids to shallow discharge zones; and (2) the drop in pressure and temperature due to erosional exhumation or upward fluid flow along faults resulted in sudden gas exsolution from reducing fluids.

Activation of a Regional Groundwater Flow System

One possible mechanism to explain the flow of reduced fluids during rapid erosional exhumation is the formation of steep topography that changed the patterns and fluxes in a regional groundwater flow system, whereby deep

meteoric water circulation flushed reduced fluids to shallow discharge zones. The development of high-relief topography in the Paradox Basin could have initiated meteoric groundwater circulation by 3–4 Ma which flushed natural gas and reducing brines through the Moab Member sandstone, bleaching red-bed sandstones along the flow paths, and possibly precipitated Mn-oxides along discharge zones (Fig. 3). To evaluate the role of topography in driving flow of reduced fluids specifically at 3.6 Ma, we need to evaluate: (1) the topographic and hydraulic gradients pre- and post-exhumation, (2) meteoric recharge locations and flow paths, and (3) how quickly reduced fluids flowed to the Moab Member sandstone in the study area.

Hydraulic Gradients and Sites of Meteoric Recharge

The presence of low-permeability confining units such as the Mancos Shale can impede meteoric water infiltration and reduce flow rates, whereas the removal of such layers can increase circulation rates (Neuzil, 1986; Tóth, 1999). An increase in topographic relief and hydraulic gradient may have coincided with removal of the Mancos Shale as erosion progressed if erosion was spatially heterogeneous (Pederson et al., 2002b). The modern-day horizontal hydraulic gradient in the northern part of the Paradox Basin ranges from ~0.009 to 0.032 (Freethey and Cordy, 1991; Lowe et al., 2007), which is significantly higher than estimated hydraulic gradients of <0.001 prior to erosion (McIntosh et al., 2023). Modern-day average vertical hydraulic gradients in the Paradox Basin range from ~0.45 east of Green River to ~1 in the southern parts of the basin, which are typical across low-permeability aquitards (Freethey and Cordy, 1991).

The closest and most likely recharge area for our study sites is the Book Cliffs (Fig. 3; Freethey and Cordy, 1991; Eisinger and Lowe, 1999; Lowe et al., 2007). Recharge of groundwater into the Navajo, Entrada, Morrison, and Dakota aquifers occurs at the base of the Book Cliffs today, and groundwater flows toward the Colorado River (Figs. 2 and 3; Freethey and Cordy, 1991). Possible barriers to fluid flow from the Book Cliffs might include the Salt Valley anticline; however, the fluids were likely transported parallel to the Salt Valley anticline along the Courthouse syncline, where one of the studied Mn-oxide deposit is located. The Colorado River provides a major discharge zone for groundwater. The Moab fault system and the faults on the flanks of the Salt Valley salt wall could have provided more localized discharge areas (Fig. 3).

Groundwater Transit Times

The distance from the Book Cliffs to the studied bleached section is ~45 km. We can calculate the fluid velocity (V) using Darcy's law, where K is hydraulic conductivity, Φ is porosity, and dh/dx is the hydraulic gradient:

$$V = K \times \frac{dh}{dx} / \Phi. \tag{1}$$

Using a range of hydraulic conductivities measured from outcrop samples and specific-capacity and drill-stem tests for the Entrada Sandstone (1.7 x 10^{-5} to 3.5×10^{-7} m/s; Fassett et al., 1977; Stone, 1983; Kernodle, 1996; Eisinger and Lowe, 1999) and a porosity of 20%, it would take ~1600-81,000 yr for meteoric water recharged at the Book Cliffs to flow 45 km at a modern-day hydraulic gradient (0.01) (Fig. 12). Given that the Book Cliffs is an erosional escarpment and has been retreating over time, the distance from the Book Cliffs to our study site would have been shorter at ca. 3-4 Ma. Nevertheless, these velocities are consistent with groundwater residence times in the Glen Canyon Group (Gardner, 2004; Noyes et al., 2021). Fluid transit times could be as long as 16,000 yr using a lower hydraulic gradient of 0.001. While these fluid transport times are a reasonable first-order approximation, we recognize that this assessment ignores anisotropic permeability, heterogeneous lithologies, and nonlinear flow paths. This calculation also only considers travel of water and conservative solutes. Nonetheless, unless hydraulic conductivities were extremely low and the transport distances were longer than 45 km, there should have been sufficient time for reducing fluids to be transported into the Moab Member within the duration of exhumation.

Another possibility is that meteoric waters recharged through the Moab Member sandstone locally. The Moab Member aquifer of the Curtis Formation is the dominant source of flow in the present-day Courthouse-Sevenmile spring and seep system, just 12 km south of the studied bleached Moab Member sandstone (Hurlow and Bishop, 2003). The spring-water chemistry, temperature, pH, and dissolved-oxygen content suggest recharge to the Moab Member aquifer occurs locally via infiltration through nearby outcrops of the Moab Member sandstone (Fig. 3), and travel times between the recharge areas and the springs are only ~50 yr (Hurlow and Bishop, 2003). If erosion had exposed the Moab Member in some locations by 3.6 Ma, then recharge may have been more localized with much shorter travel distances and mobilized any localized sources of hydrocarbons.

Sources of Reduced Fluids

For meteoric recharge and groundwater flow to have caused bleaching of the Moab Member sandstone in the study area, the groundwater must have entrained reducing fluids along the flow path. Reducing fluids could have been sourced from the Honaker Trail and Paradox Formations or oil and gas reservoirs hosted in Triassic, Jurassic, and Cretaceous units (Figs. 1 and 2). Kim et al. (2022a) suggested that brines from the Honaker Trail and Paradox Formations were likely major sources of reduced, saline, and acidic fluids that ascended along faults and bleached red-bed sandstones. However, the main stage of hydrocarbon generation and expulsion from source rocks likely occurred during maximum burial in the Late Cretaceous to Eocene (Nuccio and Condon, 1996), and at least one phase of bleaching by hydrocarbons in the Entrada Sandstone occurred ca. 41 Ma (Bailey et al., 2022a). Oil and gas resources have been produced from a range of stratigraphic units in the

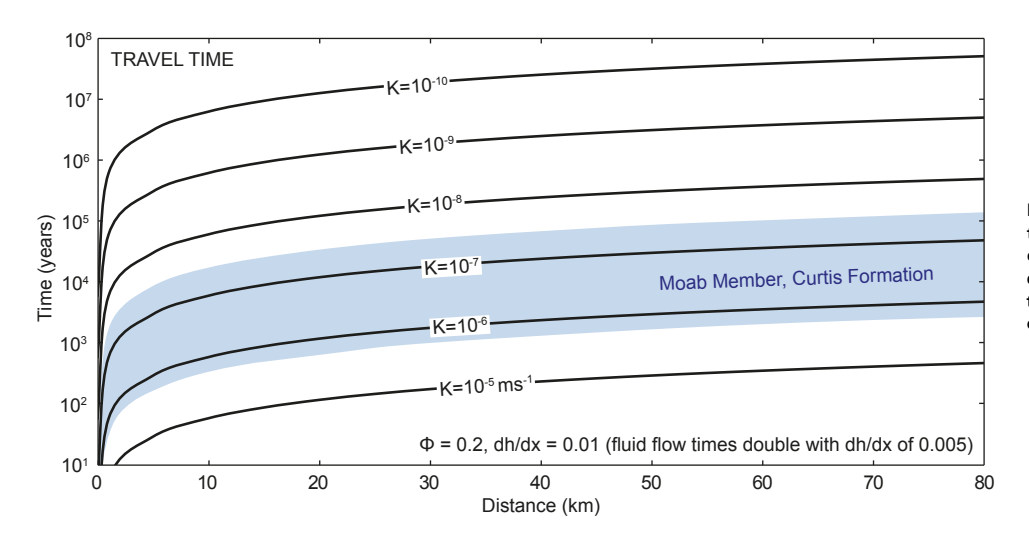


Figure 12. Time it would take for groundwater to travel distances of as much as 80 km, based on varying hydraulic conductivities (K), porosity (Φ) of 20%, and hydraulic gradient (dh/dx) of 0.01. Note that even for the longest distance, there is sufficient time for reducing fluids to have reached our study site within the duration of exhumation.

Paradox Basin, from the Pennsylvanian Honaker Trail and Paradox Formations themselves to Triassic, Jurassic (Navajo and Entrada Sandstones and Morrison Formation), and even Cretaceous units (Burro Canyon Formation, Dakota Formation, and Mancos Shale) (Fig. 1; Whidden et al., 2014).

Kim et al. (2022b) showed that deep (as deep as 3 km) groundwater flow was activated by ca. 1.1 Ma, but residual brines remain partially flushed or are still retained in evaporite confining units. Therefore, at 3.6 Ma it is unlikely that regional groundwater flow was responsible for transporting reduced fluids from as deep as the Honaker Trail Formation to the Moab Member sandstone. However, as erosion of the Colorado Plateau progressed, the depth of meteoric water circulation would have increased as Colorado River incision created lower discharge points over time. So, although meteoric water circulation may not have reached the Honaker Trail Formation by 3.6 Ma, it is plausible that groundwater was circulating in shallower formations such as the Jurassic Navajo or Entrada Sandstones and Cretaceous Dakota Formation by this time. Groundwater could have become reduced by interaction with pre-existing oil and gas reservoirs hosted in these formations and flushed reducing fluids toward discharge zones such as the Colorado River (Fig. 3; Loope et al., 2010). Unfortunately, we cannot constrain the source of the reducing fluids further without more investigation.

Amount and Composition of Reductant Required to Bleach the Curtis Formation

The bleached part of the Moab Member sandstone in our study area has an exposed area of ~554,000 m² and a thickness of ~6 m. The $\rm Fe_2O_3$ concentration decreases from 0.75% in the red sandstone to 0.24% in the bleached sandstone, requiring a reduced fluid to have removed ~0.51% of $\rm Fe_2O_3$. This

amounts to a minimum estimate of 3.4×10^7 kg of Fe₂O₃ that needs to have been dissolved by reducing fluids. Assuming the Moab Member sandstone has a porosity of 20% (Antonellini, 1992) and a density of 2.5 g/cm³ (Joesting et al., 1966), 8.5×10^5 kg of CH₄ would have been required to bleach the Moab Member sandstone based on simple stoichiometry (CH₄ + 4Fe₂O₃ + 16H⁺ = $10\text{H}_2\text{O} + \text{CO}_2 + 8\text{Fe}^{2+}$) (Chan et al., 2000). Alternatively, reaction of a CO₂-and-CH₄-bearing fluid with hematite was modeled using PHREEQC by Wigley et al. (2012), and by using their calculated stoichiometric equation ($20\text{Fe}_2\text{O}_3 + 5\text{CH}_4 + 64\text{CO}_2 + 19\text{H}_2\text{O} + 11\text{H}^+ = 30\text{Fe}^{2+} + 10\text{FeHCO}_3^+ + 59\text{HCO}_3^-$), the same volume of CH₄ as above would have been required given that the molar ratio Fe₂O₃ to CH₄ is equivalent. This would translate to ~0.8–0.5 pore volumes at temperatures <100 °C and pressures <30 MPa. Given the groundwater transit times calculated above, a minimum of 4.9 pore volumes of CH₄-saturated fluid could have passed through the Moab Member sandstone between 4 and 3.6 Ma.

Methane is not the only possible reductant for the upper Moab Member. The presence of oxidized pyrite cubes at the base of the bleached section suggests that sulfur was also available in fluids responsible for bleaching. Bacterial and thermochemical sulfate reduction of hydrocarbons has resulted in relatively high H_2S concentrations (as high as 8.5 mmol/L) in both deep and shallow brines in the Paradox Basin (Kim et al., 2022a). Experimental studies suggest H_2S is a major bleaching agent for red-bed sandstones (Moulton, 1926; Purser et al., 2014; Rushton et al., 2020). Rushton et al. (2020) suggested that H_2S was the main reducing agent for bleaching of the Entrada Sandstone in the Salt Wash graben area near Green River ($2H_2S + Fe_2O_3 + 2H^+ = FeS_2 + 3H_2O + Fe^{2+}$). Using the same rock volume, porosity, and Fe_2O_3 concentration as above, we calculate that 1.5×10^7 kg of H_2S would have been required to bleach the sandstone. However, the solubility of H_2S in water is much higher than that of CH_4 , and fewer pore volumes may have been required overall

(Carroll and Mather, 1989; Cheng et al., 2021). It is likely that both CH₄ and H₂S were present in the reducing fluids responsible for bleaching.

Gas Exsolution Induced by Decreasing Pressure and Temperature

Organic-rich shales of the Paradox Formation are thought to be the main source rocks for large quantities of both oil and gas, now produced from fields hosted in a range of reservoir units from younger and stratigraphically higher Cretaceous to Permian formations as well as deeper Mississippian formations (Nuccio and Condon, 1996; Rasmussen and Rasmussen, 2009; Whidden et al., 2014). Gas fields contain, on average, 66 mol% methane and as much as 1 mol% hydrogen sulfide (Chidsey, 2009; Kim, 2022). Many of the gas fields contain water (Kim, 2022; Kim et al., 2022a), and some portion of the gases are dissolved in the water phase. The solubility of methane decreases with decreasing pressure, decreasing temperature, and increasing salinity (Doré and Jensen, 1996; Cramer et al., 2002). At a constant pressure, methane solubility reaches a minimum at ~60 °C (Cramer et al., 2002; Duan and Mao, 2006). In the study area, meteoric water that recharged at higher elevations could have intersected oil and gas reservoirs hosted in Cretaceous and Jurassic units and become reduced prior to discharge along fault zones or the Colorado River. The decrease in pressure experienced by the reducing groundwater as it flowed up-dip toward the discharge zones could have caused exsolution of the dissolved gases (Fig. 2B). Additionally, the consequent decrease in pressure and temperature resulting from rapid erosional exhumation of this region should have liberated methane as a free gas phase. A similar process has been proposed as a mechanism of gas accumulation in West Siberia (Cramer et al., 1999, 2002) and Norway (Doré and Jensen, 1996). In fact, it has been hypothesized that major basin-centered gas fields in exhumed basins such as the nearby San Juan and Denver Basins were also derived from gas exsolution (Doré et al., 2002). The gas deposits of the Uinta and Piceance Basins, neighboring the Paradox Basin, are also considered to have formed from the exsolution of gas from pore water due to decompression during exhumation (Price, 2002).

If gas exsolution from reservoir brines during rapid exhumation of the Colorado Plateau was an important source of reduced fluids responsible for red-bed bleaching at 3.6 Ma, this raises the question of how much methane may have been exsolved during exhumation and whether it was sufficient to bleach the Curtis Formation.

Methane Released from Exsolution during Exhumation

The CH₄-and-H₂S-containing fluids responsible for bleaching were likely sourced from Cretaceous or Jurassic reservoir rocks. For the purposes of calculating methane released from exsolution during exhumation, we use the Navajo Sandstone as the source of the reducing fluids. The Navajo Sandstone has been proposed to have been one of the world's largest hydrocarbon

reservoirs before being breached by Neogene erosion (Beitler et al., 2003). In the Escalante anticline, west of the Paradox Basin, the Navajo Sandstone currently hosts as much as 110 km³ of $\rm CO_2$ and $\rm CH_4$ gas (Loope et al., 2010). We assume that prior to exhumation, the Navajo Sandstone was at a depth of 3050 m in the study area and a temperature of 100 °C and that fluids within it were at a hydrostatic pressure of 30 MPa based on burial and thermal curves constructed by Nuccio and Condon (1996). Assuming the fluids were fully saturated with respect to $\rm CH_4$, erosional exhumation of as much as 2000 m would have exsolved ~1.0–1.5 g $\rm CH_4/L$ (Cramer et al., 2002).

To exsolve enough CH_4 sufficient for bleaching, $\sim 8.5 \times 10^8$ L of CH_4 -saturated fluid hosted in the Navajo Sandstone would have been required. Assuming the Navajo Sandstone has a porosity of 20% (Parry et al., 2007), then a minimum of 0.004 km³ of rock would have been required to host that amount of fluid. Less fluid would have been required if it contained H_2S in addition to being close to saturation with CH_4 ; however, full saturation would have been unlikely. It is estimated that the Escalante anticline holds at least 42 km³ of gas, with only 0.4%-0.7% being CH_4 (Loope et al., 2010). If the exsolved gas had a similar composition $(0.4\%\ CH_4)$, then $\sim 1.1\ km³$ of rock would have been required to host the CH_4 -containing fluid.

The exsolution of methane provides a mechanism for gas to migrate upwards by buoyancy forces driven by lower gas densities with respect to other fluids such as groundwater, which could explain the observation of bleaching at the top of the Moab Member sandstone (Falta et al., 2013; Zuo et al., 2017). Fluid velocities due to buoyancy forces can be greater than topographically driven flow if the potentiometric slopes are low enough (Yang et al., 2010), which could be the case if erosional exhumation is sufficiently spatially uniform so that topographic gradients are relatively low. This would have prevented accumulating gas from being flushed from the Moab Member before sandstone bleaching could occur. The presence of a near-surface low-permeability layer, such as the Mancos Shale, can also reduce the effect of surface topography and allow buoyancy-driven fluid velocities to remain relatively high. However, regional aguitards present in the Paradox Basin today do not seem to limit flow rates of underlying aquifers (Freethey and Cordy, 1991), and the relative permeability of exsolved gas and coexisting water phases is drastically reduced in the presence of exsolved gas (Parnell, 2002; Zuo et al., 2013, 2017; Falta et al., 2013). This is because during exsolution, the gas phase appears as disconnected bubbles, and pore throat diameters of the porous rock would need to be larger than the gas bubble to allow gas migration (Khilyuk et al., 2000). Nevertheless, in high-permeability systems at shallow depths such as the Moab Member sandstone during exhumation, the density contrast between the brine and gas phases would be large enough to allow exsolved gas to exhibit some mobility through the sandstones (Falta et al., 2013).

Pathways of Gas Migration from Deeper Formations

Volumetric expansion of the gaseous petroleum phases in the source rocks during exhumation can also drive late-stage primary migration, resulting in

the discharge of additional petroleum into reservoir formations ("exhumation charge;" English et al., 2016a). Gas exsolution from deep brines or "exhumation charge" of gas from source rocks could provide a mechanism for CH₄ migration upwards into the Moab Member sandstone. Increased pore volume and poroelastic expansion in the aquifer due to decreased pressure would be minor, with more significant expansion occurring in the shale source rocks at greater depths due to the low compressibility of sandstone (Corbet and Bethke, 1992). In our study area, multiple faults and other steep high-permeability gradients associated with lithologic contacts and salt deformation form likely migration pathways for exsolved gases and reducing fluids.

Similarly, fluid flow along fault zones would be triggered by a drop in pressure in upper aquifers when outlets opened during progressive erosion. Faults and fractures form high-permeability channels that can allow large volumes of gas and brines to migrate (Khilyuk et al., 2000). During upward flow along fault zones, the drop in fluid pressure could trigger more localized exsolution of methane, which could explain the localized nature of the observed Fe- and Mn-oxides and bleaching of the Curtis Formation.

CONCLUSIONS

(U-Th)/He and K-Ar dates of Mn-oxides and clays precipitated by reducing fluids in the Moab fault and in bleached sandstones in the Moab area indicate formation between 3.6 and 3.9 Ma, similar to the previously documented ages of Fe- and Mn-oxides near other faults in the area (Garcia et al., 2018). We interpret these ages to represent a distinct phase of subsurface flow of reduced fluids and reorganization of subsurface flow systems in the Pliocene. This timing coincides with rapid erosional exhumation of ~1.5–2 km that started ca. 4 Ma (Murray et al., 2016, 2019) and, at least locally, decreased significantly by 3.6 Ma (Garcia et al., 2018). The coincidence of the timing of red-bed bleaching, formation of Mn-oxides, and timing of rapid erosional exhumation raises the question of how denudation at the surface can induce a phase of reduced fluid flow in the subsurface.

Prior to erosion, the topographic surface in the Paradox Basin was relatively flat and the hydraulic gradients low (Fig. 2A). Steep topography and higher hydraulic gradients would have formed in response to spatially heterogeneous, rapid erosional exhumation which in turn could have reorganized regional groundwater flow (Fig. 2B). The Moab Member sandstone may have been exhumed to the surface by incision by the Colorado River ca. 3.6 Ma, which opened groundwater discharge outlets and triggered a pressure drop in the sandstone aquifers (Fig. 2B). Regional groundwater flow systems can mobilize and transport reduced, hydrocarbon-bearing fluids over long distances. We suggest that meteoric water recharged at the base of the Book Cliffs interacted with shallow oil and gas reservoirs present in the Cretaceous Dakota and Cedar Mesa Formations and the Jurassic Morrison and Entrada Formations and bleached the Moab Member sandstone (Figs. 2 and 3). Groundwater flow rates would have increased following erosion and breaching of the Mancos

Shale. We estimated that it took less than 100,000 years for meteoric water recharged at the Book Cliffs to reach the studied bleached section, which is consistent with groundwater residence times in the Glen Canyon Group (Gardner, 2004; Noyes et al., 2021). The groundwater velocities were fast enough to allow several pore volumes of reducing fluids to interact with and bleach the Moab Member sandstone over the duration of exhumation. Gases were likely exsolved from the reducing groundwater as the pressure decreased along the flow path. Metals such as Fe and Mn are mobilized during flow of reduced fluids and sandstone bleaching. These metals were precipitated ca. 3.6 Ma as Fe- and Mn-oxides near redox fronts in contact with near-surface oxygenated fluids along discharge zones such as the Moab fault. The Fe- and Mn-oxides from this study likely reflect just the most recent phase of fluid migration along the Moab fault.

The decrease in pressure and temperature during and following erosional exhumation of the Colorado Plateau or during upward flow along fault zones may also have liberated gases such as methane as a free gas phase (Doré and Jensen, 1996; Cramer et al., 1999, 2002). The exsolution of gas provides a mechanism for gas-rich fluids to migrate upwards by buoyancy forces, which could explain the observation of bleaching at the top of the Moab Member sandstone below low-permeability shale of the Summerville Formation. Faults and fractures form high-permeability channels that can allow large volumes of gas and brines to migrate (Khilyuk et al., 2000).

Erosion rates slowed at least locally in the Canyonlands region by 3.6 Ma, and Fe- and Mn-oxide deposits have experienced <0.5 km of erosion since then, as suggested by Garcia et al. (2018). This rate of erosion matches the lower end of modern incision rates on the Colorado Plateau, which range from ~0.14 km/m.y. to 0.45 km/m.y. according to cosmogenic nuclide dating of fill terraces along the Colorado River (Pederson et al., 2006, 2013).

We suggest that both of the above mechanisms (regional groundwater flow and gas exsolution) were responsible for the flow of reduced fluids during rapid erosional exhumation of the Colorado Plateau. It is likely that gas exsolution and expansion due to decreasing pressure and temperature was the dominant process in the early stages of erosion when hydraulic gradients were still relatively low. As the Mancos Shale and aquifer units were breached by erosion and hydraulic gradients increased, topographically driven flow became the dominant mechanism. Meteoric water recharged at high-elevation areas such as the Book Cliffs and flushed pre-existing reducing fluids toward discharge zones. Erosion-driven flow of reduced fluids and gas exsolution may be responsible for sandstone bleaching in other areas of the Colorado Plateau.

ACKNOWLEDGMENTS

Funding for this research was provided by the William F. Keck Foundation, the U.S. National Science Foundation Division of Earth Sciences (grant 2120733), and Canadian Institute for Advanced Research (CIFAR) Earth4D: Subsurface Science and Exploration (McIntosh is a Fellow). We gratefully acknowledge Uttam Chowdhury, Mary Kay Amistadi, and Tanzhuo Liu for analytical assistance. We thank Bob Krantz for valuable field reconnoitering; Jay Quade and Dennis Newell for helpful discussions; and David Boutt, Greg Hoke, and an anonymous reviewer for very constructive and positive reviews.

REFERENCES CITED

- Adams, J.J., and Bachu, S., 2002, Equations of state for basin geofluids: Algorithm review and intercomparison for brines: Geofluids, v. 2, p. 257–271, https://doi.org/10.1046/j.1468-8123.2002.00041.x.
- Adams, J.J., Rostron, B.J., and Mendoza, C.A., 2004, Coupled fluid flow, heat and mass transport, and erosion in the Alberta basin: Implications for the origin of the Athabasca oil sands: Canadian Journal of Earth Sciences, v. 41, p. 1077–1095, https://doi.org/10.1139/e04-052.
- Antonellini, M., 1992, Geometry and distribution of deformation bands in porous sandstones, Delicate Arch area, Arches National Park, Utah: Stanford, California, Rock Fracture Project, v. 3. p. A1–A7.
- Baars, D.L., and Stevenson, G.M., 1982, Subtle stratigraphic traps in Paleozoic rocks of Paradox Basin, in Halbouty, M.T., ed., The Deliberate Search for the Subtle Trap: American Association of Petroleum Geologists Memoir 32, p. 131–158, https://doi.org/10.1306/M32427C9.
- Bailey, L.R., Drake, H., Whitehouse, M.J., and Reiners, P.W., 2022a, Characteristics and consequences of red bed bleaching by hydrocarbon migration: A natural example from the Entrada Sandstone, southern Utah: Geochemistry, Geophysics, Geosystems, v. 23, https://doi.org/10.1029/2022GC010465.
- Bailey, L.R., Kirk, J., Hemming, S.R., Krantz, R.W., and Reiners, P.W., 2022b, Eocene fault-controlled fluid flow and mineralization in the Paradox Basin, United States: Geology, v. 50, p. 326–330, https://doi.org/10.1130/G49466.1.
- Barbeau, D.L., 2003, A flexural model for the Paradox Basin: Implications for the tectonics of the Ancestral Rocky Mountains: Basin Research, v. 15, p. 97–115, https://doi.org/10.1046/j.1365 -2117.2003.00194.x.
- Barton, I.F., Barton, M.D., and Thorson, J.P., 2018a, Characteristics of Cu and U-V deposits in the Paradox Basin (Colorado Plateau) and associated alteration, in Thorson, J.P., ed., Paradox Basin Fluids and Colorado Plateau Copper, Uranium, and Vanadium Deposits Field Trip: Society of Economic Geologists Guidebook 59, p. 73–102.
- Barton, M.D., Barton, I.F., and Thorson, J.P., 2018b, Paleofluid flow in the Paradox Basin: Introduction, *in* Thorson, J.P., ed., Paradox Basin Fluids and Colorado Plateau Copper, Uranium, and Vanadium Deposits Field Trip: Society of Economic Geologists Guidebook 59, p. 1–12.
- Beitler, B., Chan, M.A., and Parry, W.T., 2003, Bleaching of Jurassic Navajo Sandstone on Colorado Plateau Laramide highs: Evidence of exhumed hydrocarbon supergiants?: Geology, v. 31, p. 1041–1044, https://doi.org/10.1130/G19794.1.
- Beitler, B., Parry, W.T., and Chan, M.A., 2005, Fingerprints of fluid flow: Chemical diagenetic history of the Jurassic Navajo Sandstone, southern Utah, U.S.A.: Journal of Sedimentary Research, v. 75, p. 547–561, https://doi.org/10.2110/jsr.2005.045.
- Bethke, C.M., 1985, A numerical model of compaction-driven groundwater flow and heat transfer and its application to the paleohydrology of intracratonic sedimentary basins: Journal of Geophysical Research: Solid Earth, v. 90, p. 6817–6828, https://doi.org/10.1029/JB090iB08p06817.
- Bethke, C.M., and Marshak, S., 1990, Brine migrations across North America—The plate tectonics of groundwater: Annual Review of Earth and Planetary Sciences, v. 18, p. 287–315, https://doi.org/10.1146/annurev.ea.18.050190.001443.
- Bethke, C.M., Reed, J.D., and Oltz, D.F., 1991, Long-range petroleum migration in the Illinois Basin: American Association of Petroleum Geologists Bulletin, v. 75, p. 925–945, https://doi.org/10.1306/0C9B2899-1710-11D7-8645000102C1865D.
- Birkholzer, J.T., and Zhou, Q., 2009, Basin-scale hydrogeologic impacts of CO₂ storage: Capacity and regulatory implications: International Journal of Greenhouse Gas Control, v. 3, p. 745–756, https://doi.org/10.1016/j.ijggc.2009.07.002.
- Bjørlykke, K., 1999, Principal aspects of compaction and fluid flow in mudstones, in Aplin, A.C., Fleet, A.J., and MacQuaker, J.H.S., eds., Muds and Mudstones: Physical and Fluid-Flow Properties: Geological Society of London Special Publication 158, p. 73–78, https://doi.org/10.1144/GSL.SP.1999.158.01.06.
- Bjørlykke, K., and Høeg, K., 1997, Effects of burial diagenesis on stresses, compaction and fluid flow in sedimentary basins: Marine and Petroleum Geology, v. 14, p. 267–276, https://doi .org/10.1016/S0264-8172(96)00051-7.
- Blanchard, P.J., 1990, Ground-Water Conditions in the Grand Country Area, Utah, with Emphasis on the Mill-Creek Spanish Valley Area: U.S. Geological Survey Technical Publication 100, 77 p.
- Bump, A.P., and Davis, G.H., 2003, Late Cretaceous–early Tertiary Laramide deformation of the northern Colorado Plateau, Utah and Colorado: Journal of Structural Geology, v. 25, p. 421–440, https://doi.org/10.1016/S0191-8141(02)00033-0.
- Bursztyn, N., Pederson, J.L., Tressler, C., Mackley, R.D., and Mitchell, K.J., 2015, Rock strength along a fluvial transect of the Colorado Plateau—Quantifying a fundamental control on

- geomorphology: Earth and Planetary Science Letters, v. 429, p. 90–100, https://doi.org/10.1016/j.epsl.2015.07.042.
- Carroll, J.J., and Mather, A.E., 1989, The solubility of hydrogen sulphide in water from 0 to 90°C and pressures to 1 MPa: Geochimica et Cosmochimica Acta, v. 53, p. 1163–1170, https://doi.org/10.1016/0016-7037(89)90053-7.
- Chan, M.A., Parry, W.T., and Bowman, J.R., 2000, Diagenetic hematite and manganese oxides and fault-related fluid flow in Jurassic sandstones, southeastern Utah: American Association of Petroleum Geologists Bulletin, v. 84, p. 1281–1310, https://doi.org/10.1306/A9673E82-1738 -11D7-8645000102C1865D
- Chan, M.A., Parry, W.T., Petersen, E.U., and Hall, C.M., 2001, ⁴⁰Ar/⁵⁹Ar age and chemistry of manganese mineralization in the Moab and Lisbon fault systems, southeastern Utah: Geology, v. 29, p. 331–334. https://doi.org/10.1130/0091-7613(2001)029<0331:AAAACO>2.0.CO:2.
- Chan, M.A., Ormö, J., Park, A.J., Stich, M., Souza-Egipsy, V., and Komatsu, G., 2007, Models of iron oxide concretion formation: Field, numerical, and laboratory comparisons: Geofluids, v. 7, p. 356–368, https://doi.org/10.1111/i.1468-8123.2007.00187.x.
- Cheng, H., Li, N., Zhang, R., Wang, N., Yang, Y., Teng, Y., Jia, W., and Zheng, S., 2021, Measuring and modeling the solubility of hydrogen sulfide in rFeCl₃/[bmim]Cl: Processes, v. 9, 652, https://doi.org/10.3390/pr9040652.
- Chidsey, T.C., Jr., ed., 2009, Major oil plays in Utah and vicinity: Final report: Utah Geological Survey. Cook, K.L., Whipple, K.X., Heimsath, A.M., and Hanks, T.C., 2009, Rapid incision of the Colorado River in Glen Canyon—Insights from channel profiles, local incision rates, and modeling of lithologic controls: Earth Surface Processes and Landforms, v. 34, p. 994–1010, https://doi.org/10.1002/esp.1790.
- Corbet, T.F., and Bethke, C.M., 1992, Disequilibrium fluid pressures and groundwater flow in the western Canada sedimentary basin: Journal of Geophysical Research: Solid Earth, v. 97, p. 7203–7217, https://doi.org/10.1029/91JB02993.
- Cramer, B., Poelchau, H.S., Gerling, P., Lopatin, N.V., and Littke, R., 1999, Methane released from groundwater: The source of natural gas accumulations in northern West Siberia: Marine and Petroleum Geology, v. 16, p. 225–244, https://doi.org/10.1016/S0264-8172(98)00085-3.
- Cramer, B., Schlömer, S., and Poelchau, H.S., 2002, Uplift-related hydrocarbon accumulations: The release of natural gas from groundwater, in Doré, A.G., Cartwright, J.A., Stoker, M.S., Turner, J.P., and White, N., eds., Exhumation of the North Atlantic Margin: Timing, Mechanisms and Implications for Petroleum Exploration: Geological Society of London Special Publication 196, p. 447–455, https://doi.org/10.1144/GSL.SP.2002.196.01.24.
- Crossey, L.C., Karlstrom, K.E., Dorsey, R., Pearce, J., Wan, E., Beard, L.S., Asmerom, Y., Polyak, V., Crow, R.S., Cohen, A., Bright, J., and Pecha, M.E., 2015, Importance of groundwater in propagating downward integration of the 6–5 Ma Colorado River system: Geochemistry of springs, travertines, and lacustrine carbonates of the Grand Canyon region over the past 12 Ma: Geosphere, v. 11, p. 660–682. https://doi.org/10.1130/GES01073.1.
- Crow, R.S., Schwing, J., Karlstrom, K.E., Heizler, M., Pearthree, P.A., House, P.K., Dulin, S., Jänecke, S.U., Stelten, M., and Crossey, L.J., 2021, Redefining the age of the lower Colorado River, southwestern United States: Geology, v. 49, p. 635–640, https://doi.org/10.1130/G48080.1.
- Cui, T., Yang, J., and Samson, I.M., 2012, Tectonic deformation and fluid flow: Implications for the formation of unconformity-related uranium deposits: Economic Geology, v. 107, p. 147–163, https://doi.org/10.2113/econgeo.107.1.147.
- Cumberland, S.A., Douglas, G., Grice, K., and Moreau, J.W., 2016, Uranium mobility in organic matter-rich sediments: A review of geological and geochemical processes: Earth-Science Reviews, v. 159, p. 160–185, https://doi.org/10.1016/j.earscirev.2016.05.010.
- Darling, A.L., Karlstrom, K.E., Granger, D.E., Aslan, A., Kirby, E., Ouimet, W.B., Lazear, G.D., Coblentz, D.D., and Cole, R.D., 2012, New incision rates along the Colorado River system based on cosmogenic burial dating of terraces: Implications for regional controls on Quaternary incision: Geosphere, v. 8, p. 1020–1041, https://doi.org/10.1130/GES00724.1.
- Doelling, H.H., 2002, Geologic map of the Moab and eastern part of the San Rafael Desert 30' x 60' quadrangles, Grand and Emery Counties, Utah, and Mesa County, Colorado: Utah Geological Survey Geological Map 180, scale 1:100,000.
- Doré, A.G., and Jensen, L.N., 1996, The impact of late Cenozoic uplift and erosion on hydrocarbon exploration: Offshore Norway and some other uplifted basins: Global and Planetary Change, v. 12, p. 415–436, https://doi.org/10.1016/0921-8181(95)00031-3.
- Doré, A.G., Corcoran, D.V., and Scotchman, I.C., 2002, Prediction of the hydrocarbon system in exhumed basins, and application to the NW European margin, *in* Dore, A.G., Cartwright, J.A., Stoker, M.S., Turner, J.P., and White, N., eds., Exhumation of the North Atlantic Margin: Timing,

- Mechanisms and Implications for Petroleum Exploration: Geological Society of London Special Publication 196, p. 401–429, https://doi.org/10.1144/GSL.SP.2002.196.01.21.
- Duan, Z., and Mao, S., 2006, A thermodynamic model for calculating methane solubility, density and gas phase composition of methane-bearing aqueous fluids from 273 to 523K and from 1 to 2000bar: Geochimica et Cosmochimica Acta, v. 70, p. 3369–3386, https://doi.org/10.1016/j.gca.2006.03.018.
- Eichhubl, P., Davatzes, N.C., and Becker, S.P., 2009, Structural and diagenetic control of fluid migration and cementation along the Moab fault, Utah: American Association of Petroleum Geologists Bulletin, v. 93, p. 653–681, https://doi.org/10.1306/02180908080.
- Eisinger, C., and Lowe, M., 1999, A summary of the ground-water resources and geohydrology of Grand County. Utah: Utah Geological Survey Circular 99, 19 p., https://doi.org/10.34191/C-99.
- English, J.M., English, K.L., Corcoran, D.V., and Toussaint, F., 2016a, Exhumation charge: The last gasp of a petroleum source rock and implications for unconventional shale resources: American Association of Petroleum Geologists Bulletin, v. 100, p. 1–16, https://doi.org/10 .1306/07271514224.
- English, K.L., English, J.M., Redfern, J., Hollis, C., Corcoran, D.V., Oxtoby, N., and Yahia Cherif, R., 2016b, Remobilization of deep basin brine during exhumation of the Illizi Basin, Algeria: Marine and Petroleum Geology, v. 78, p. 679–689, https://doi.org/10.1016/j.marpetgeo.2016.08.016.
- Falta, R.W., Zuo, L., and Benson, S.M., 2013, Migration of exsolved CO₂ following depressurization of saturated brines: Greenhouse Gases: Science and Technology, v. 3, p. 503–515, https://doi.org/10.1002/ghg.1379.
- Fan, Y., Duffy, C.J., and Oliver, D.S., Jr., 1997, Density-driven groundwater flow in closed desert basins: Field investigations and numerical experiments: Journal of Hydrology (Amsterdam), v. 196, p. 139–184, https://doi.org/10.1016/S0022-1694(96)03292-1.
- Fassett, J.E., Jentgen, R.W., Black, B.A., Molenaar, C.M., and Woodward, L.A., 1977, Second Day— Road log from Red Mountain oil field to El Vado Lake via Pueblo, Pintado, Star Lake, Torreon, Cuba and Llaves, *in* Fassett, J.E., and James, H.L., eds., San Juan Basin III: Northwestern New Mexico: New Mexico Geological Society 28th Annual Fall Field Conference Guidebook, p. 19–38.
- Ferguson, G., McIntosh, J.C., Grasby, S.E., Hendry, M.J., Jasechko, S., Lindsay, M.B.J., and Luijendijk, E., 2018, The persistence of brines in sedimentary basins: Geophysical Research Letters, v. 45, p. 4851–4858, https://doi.org/10.1029/2018GL078409.
- Fleming, R.F., 1994, Cretaceous pollen in Pliocene rocks: Implications for Pliocene climate in the southwestern United States: Geology, v. 22, p. 787–790, https://doi.org/10.1130/0091-7613 (1994)022<0787:CPIPRI>2.3.CO;2.
- Freethey, G.W., and Cordy, G.E., 1991, Geohydrology of Mesozoic rocks in the upper Colorado River basin in Arizona, Colorado, New Mexico, Utah, and Wyoming, excluding the San Juan Basin: U.S. Geological Survey Professional Paper 1411-C, 118 p., 6 plates, https://doi.org/10.3133/pp1411C.
- Freeze, R.A., and Cherry, J.A., 1979, Groundwater: Englewood Cliffs, New Jersey, Prentice-Hall Inc., 604 p.
- Freeze, R.A., and Witherspoon, P.A., 1967, Theoretical analysis of regional groundwater flow: 2. Effect of water-table configuration and subsurface permeability variation: Water Resources Research, v. 3, p. 623–634, https://doi.org/10.1029/WR003i002p00623.
- Garcia, V.H., Reiners, P.W., Shuster, D.L., Idleman, B., and Zeitler, P.K., 2018, Thermochronology of sandstone-hosted secondary Fe- and Mn-oxides near Moab, Utah: Record of paleo-fluid flow along a fault: Geological Society of America Bulletin, v. 130, p. 93–113, https://doi.org/10.1130/B316271.
- Garden, I.R., Guscott, S.C., Burley, S.D., Foxford, K.A., Walsh, J.J., and Marshall, J., 2001, An exhumed palaeo-hydrocarbon migration fairway in a faulted carrier system, Entrada Sandstone of SE Utah, USA: Geofluids, v. 1, p. 195–213, https://doi.org/10.1046/j.1468-8123.2001.00018.x.
- Gardner, P.M., 2004, Environmental tracer investigation of groundwater conditions at the Scott M. Matheson Wetland Preserve near Moab, Utah [M.S. thesis]: Salt Lake City, Utah, University of Utah, 160 p.
- Garven, G., 1989, A hydrogeologic model for the formation of the giant oil sands deposits of the Western Canada sedimentary basin: American Journal of Science, v. 289, p. 105–166, https:// doi.org/10.2475/ajs.289.2.105.
- Garven, G., 1995, Continental-scale groundwater flow and geologic processes: Annual Review of Earth and Planetary Sciences, v. 23, p. 89–117, https://doi.org/10.1146/annurev.ea.23 .050195.000513.
- Gorenc, M.A., and Chan, M.A., 2015, Hydrocarbon-induced diagenetic alteration of the Permian White Rim Sandstone, Elaterite Basin, southeast Utah: American Association of Petroleum Geologists Bulletin, v. 99, p. 807–829, https://doi.org/10.1306/10081413128.

- Guerrero, J., Bruhn, R.L., McCalpin, J.P., Gutiérrez, F., Willis, G., and Mozafari, M., 2015, Salt-dissolution faults versus tectonic faults from the case study of salt collapse in Spanish Valley, SE Utah (USA): Lithosphere, v. 7, p. 46–58, https://doi.org/10.1130/L385.1.
- Gvirtzman, H., and Stanislavsky, E., 2000, Palaeohydrology of hydrocarbon maturation, migration and accumulation in the Dead Sea Rift: Basin Research, v. 12, p. 79–93, https://doi.org/10.1046/j.1365-2117.2000.00111.x.
- Hahn, G.A., and Thorson, J.P., 2005, Geology of the Lisbon Valley sandstone-hosted disseminated copper deposits, San Juan County, Utah, in Thorson, J.P., ed., Lisbon Valley Sediment-Hosted Copper Deposits and Paradox Basin Fluids Trip: Society of Economic Geologists Guidebook 37, p. 19–42, https://doi.org/10.5382/GB.37.ch3.
- Haitjema, H.M., and Mitchell-Bruker, S., 2005, Are water tables a subdued replica of the topography?: Ground Water, v. 43, p. 781–786, https://doi.org/10.1111/j.1745-6584.2005.00090.x.
- Herrmann, W., and Berry, R.F., 2002, MINSQ—A least squares spreadsheet method for calculating mineral proportions from whole rock major element analyses: Geochemistry: Exploration, Environment, Analysis, v. 2, p. 361–368, https://doi.org/10.1144/1467-787302-010.
- Hite, R.J., Anders, D.E., and Ging, T.G., 1984, Organic-rich source rocks of Pennsylvanian age in the Paradox Basin of Utah and Colorado, in Woodward, J., Meissner, F.F., and Clayton, J.L. eds., Hydrocarbon Source Rocks of the Greater Rocky Mountain Region: Denver, Colorado, Rocky Mountain Association of Geologists, p. 255–274.
- Hoffman, M., Stockli, D.F., Kelley, S.A., Pederson, J., and Lee, J., 2010, Mio-Pliocene erosional exhumation of the central Colorado Plateau, eastern Utah – New insights from apatite (U-Th)/ He thermochronometry, in Beard, L.S., Karlstrom, K.E., Young, R.A., and Billingsley, G.H., eds., CRevolution 2—Origin and Evolution of the Colorado River System, Workshop Abstracts: U.S. Geological Survey Open-File Report 2011-1210, p. 132–135.
- Hubbert, M.K., 1953, Entrapment of petroleum under hydrodynamic conditions: American Association of Petroleum Geologists Bulletin, v. 37, p. 1954–2026, https://doi.org/10.1306 /5CEADD61-16BB-11D7-8645000102C1865D.
- Hunt, C.B., 1956, Cenozoic geology of the Colorado Plateau: U.S. Geological Survey Professional Paper 279, 97 p., https://doi.org/10.3133/pp279.
- Hurlow, H.A., and Bishop, C.E., 2003, Recharge areas and geologic controls for the Courthouse-Sevenmile spring system, Western Arches National Park, Grand County, Utah: Utah Geological Survey Special Study 108, 56 p., https://doi.org/10.34191/SS-108.
- Iverson, N., and Person, M., 2012, Glacier-bed geomorphic processes and hydrologic conditions relevant to nuclear waste disposal: Geofluids, v. 12, p. 38–57, https://doi.org/10.1111/j.1468-8123.2011.00355.x.
- Jochems, A.P., and Pederson, J.L., 2015, Active salt deformation and rapid, transient incision along the Colorado River near Moab, Utah: Journal of Geophysical Research: Earth Surface, v. 120, p. 730–744, https://doi.org/10.1002/2014JF003169.
- Joesting, H.R., Case, J.E., and Plouff, D., 1966, Regional geophysical investigations of the Moab-Needles area, Utah: U.S. Geological Survey Professional Paper 516-C, 21 p., https:// doi.org/10.3133/pp516C.
- Johnson, D.M., Hooper, P.R., and Conrey, R.M., 1999, XRF analysis of rocks and minerals for major and trace elements on a single low dilution Li-tetraborate fused bead: JCPDS-International Centre for Diffraction Data, p. 843–867.
- Karlstrom, K.E., Coblentz, D., Dueker, K., Ouimet, W., Kirby, E., Van Wijk, J., Schmandt, B., Kelley, S., Lazear, G., Crossey, L.J., Crow, R., Aslan, A., Darling, A., Aster, R., MacCarthy, J., Hansen, S.M., Stachnik, J., Stockli, D.F., Garcia, R.V., Hoffman, M., McKeon, R., Feldman, J., Heizler, M., Donahue, M.S., and the CREST Working Group, 2012, Mantle-driven dynamic uplift of the Rocky Mountains and Colorado Plateau and its surface response: Toward a unified hypothesis: Lithosphere, v. 4, p. 3–22, https://doi.org/10.1130/L150.1.
- Karlstrom, K.E., Lee, J.P., Kelley, S.A., Crow, R.S., Crossey, L.J., Young, R.A., Lazear, G., Beard, L.S., Ricketts, J.W., Fox, M., and Shuster, D.L., 2014, Formation of the Grand Canyon 5 to 6 million years ago through integration of older palaeocanyons: Nature Geoscience, v. 7, p. 239–244, https://doi.org/10.1038/ngeo2065.
- Kernodle, J.M., 1996, Hydrogeology and steady-state simulation of ground-water flow in the San Juan Basin, New Mexico, Colorado, Arizona, and Utah: U.S. Geological Survey Water-Resources Investigations Report 95-4187, 117 p., https://doi.org/10.3133/wri954187.
- Kettler, R.M., Loope, D.B., and Weber, K.A., 2011, Follow the water: Connecting a CO₂ reservoir and bleached sandstone to iron-rich concretions in the Navajo Sandstone of south-central Utah, USA: Reply: Geology, v. 39, p. e251–e252, https://doi.org/10.1130/G32550Y.1.
- Khilyuk, L.F., Chilingar, G.V., Robertson, J.O., Jr., and Endres, B., 2000, Gas Migration: Events Preceding Earthquakes: Houston, Texas, Gulf Publishing Company, 389 p., https://doi.org/10.1016/B978-0-88415-430-3.X5000-9.

- Kim, J., 2022, Hydrogeochemical evolution of basinal fluids in the Paradox Basin: Implications for sources, paleofluid flow, residence time, and water-rock-gas-microbe interactions [Ph.D. thesis]: Tucson, Arizona, University of Arizona, 191 p.
- Kim, J.-H., Bailey, L., Noyes, C., Tyne, R.L., Ballentine, C.J., Person, M., Ma, L., Barton, M., Barton, I., Reiners, P.W., Ferguson, G., and McIntosh, J., 2022a, Hydrogeochemical evolution of formation waters responsible for sandstone bleaching and ore mineralization in the Paradox Basin, Colorado Plateau, USA: Geological Society of America Bulletin, v. 134, p. 2589–2610, https://doi.org/10.1130/B36078.1.
- Kim, J.-H., Ferguson, G., Person, M., Jiang, W., Lu, Z.-T., Ritterbusch, F., Yang, G.-M., Tyne, R., Bailey, L., Ballentine, C., Reiners, P., and McIntosh, J., 2022b, Krypton-81 dating constrains timing of deep groundwater flow activation: Geophysical Research Letters, v. 49, https:// doi.org/10.1029/2021GL097618.
- Koons, P.O., Craw, D., Cox, S.C., Upton, P., Templeton, A.S., and Chamberlain, C.P., 1998, Fluid flow during active oblique convergence: A Southern Alps model from mechanical and geochemical observations: Geology, v. 26, p. 159–162, https://doi.org/10.1130/0091-7613(1998) 026-0159:FFDAOC>2.3.CO:2.
- Krevor, S., de Coninck, H., Gasda, S.E., Ghaleigh, N.S., de Gooyert, V., Hajibeygi, H., Juanes, R., Neufeld, J., Roberts, J.J., and Swennenhuis, F., 2023, Subsurface carbon dioxide and hydrogen storage for a sustainable energy future: Nature Reviews Earth & Environment, v. 4, p. 102–118, https://doi.org/10.1038/s43017-022-00376-8.
- Lazear, G., Karlstrom, K., Aslan, A., and Kelley, S., 2013, Denudation and flexural isostatic response of the Colorado Plateau and southern Rocky Mountains region since 10 Ma: Geosphere, v. 9, p. 792–814, https://doi.org/10.1130/GES00836.1.
- Loope, D.B., Kettler, R.M., and Weber, K.A., 2010, Follow the water: Connecting a CO₂ reservoir and bleached sandstone to iron-rich concretions in the Navajo Sandstone of south-central Utah, USA: Geology, v. 38, p. 999–1002, https://doi.org/10.1130/G31213.1.
- Loope, D.B., Kettler, R.M., Weber, K.A., Hinrichs, N.L., and Burgess, D.T., 2012, Rinded iron-oxide concretions: Hallmarks of altered siderite masses of both early and late diagenetic origin: Sedimentology, v. 59, p. 1769–1781, https://doi.org/10.1111/j.1365-3091.2012.01325.x.
- Lowe, M., Wallace, J., Kirby, S.M., and Bishop, C.E., 2007, The hydrogeology of Moab-Spanish Valley, Grand and San Juan Counties, Utah, with emphasis on maps for water-resource management and land-use planning: Utah Geological Survey Special Study 120, 40 p.
- Lucchitta, I., 1972, Early history of the Colorado River in the Basin and Range province: Geological Society of America Bulletin, v. 83, p. 1933–1948, https://doi.org/10.1130/0016-7606(1972)83[1933:EHOTCR]2.0.CO;2.
- MacIntyre, T.J., Hitzman, M.W., and Thorson, J.P., 2023, Hydrocarbon-induced bleaching and copper mineralization in the Wingate Sandstone, Paradox Valley, Colorado: Two episodes of fluid migration during the evolution of the Paradox Basin: American Association of Petroleum Geologists Bulletin, v. 107, p. 169–189, https://doi.org/10.1306/08042221112.
- Marklund, L., and Wörman, A., 2007, The impact of hydraulic conductivity on topography driven groundwater flow, *in* Rowiński, P.M. ed., Transport Phenomena in Hydraulics: Publications of the Institute of Geophysics, Polish Academy of Sciences, v. E-7, p. 159–167.
- Mauch, J.P., 2018, Quaternary incision, salt tectonism, and landscape evolution of Moab-Spanish Valley, Utah [M.S. thesis]: Logan, Utah, Utah State University, 235 p., https://doi.org/10.26076/5ec4-edf5.
- Maxwell, R.M., and Kollet, S.J., 2008, Interdependence of groundwater dynamics and land-energy feedbacks under climate change: Nature Geoscience, v. 1, p. 665–669, https://doi.org/10.1038/ngeo315.
- McCarroll, N.R., 2019, Evolution of the Book Cliffs dryland escarpment in central Utah—Establishing rates and testing models of escarpment retreat [M.S. thesis]: Logan, Utah, Utah State University, 137 p., https://doi.org/10.26076/a6c0-e711.
- McIntosh, J.C., and Ferguson, G., 2021, Deep meteoric water circulation in Earth's crust: Geophysical Research Letters, v. 48, https://doi.org/10.1029/2020GL090461.
- McIntosh, J., Kim, J.-H., Bailey, L., Osburn, M., Drake, H., Martini, A., Reiners, P., Stevenson, B., and Ferguson, G., 2023, Burial and denudation alter microbial life at the bottom of the hypo-critical zone: Geochemistry, Geophysics, Geosystems, v. 24, https://doi.org/10.1029/2022GC010831.
- McLellan, J.G., Oliver, N.H.S., and Schaubs, P.M., 2004, Fluid flow in extensional environments: Numerical modelling with an application to Hamersley iron ores: Journal of Structural Geology, v. 26, p. 1157–1171, https://doi.org/10.1016/j.jsg.2003.11.015.
- Moulton, G.F., 1926, Some features of redbed bleaching: American Association of Petroleum Geologists Bulletin, v. 10, p. 304–311, https://doi.org/10.1306/3D932715-16B1-11D7 -8645000102C1865D.

- Murray, K.E., Reiners, P.W., and Thomson, S.N., 2016, Rapid Pliocene–Pleistocene erosion of the central Colorado Plateau documented by apatite thermochronology from the Henry Mountains: Geology, v. 44, p. 483–486, https://doi.org/10.1130/G37733.1.
- Murray, K.E., Reiners, P.W., Thomson, S.N., Robert, X., and Whipple, K.X., 2019, The ther-mochronologic record of erosion and magmatism in the Canyonlands region of the Colorado Plateau: American Journal of Science, v. 319, p. 339–380, https://doi.org/10.2475/05.2019.01.
- Nelson, S.T., Davidson, J.P., and Sullivan, K.R., 1992, New age determinations of central Colorado Plateau laccoliths, Utah: Recognizing disturbed K-Ar systematics and re-evaluating tectonomagmatic relationships: Geological Society of America Bulletin, v. 104, p. 1547–1560, https://doi.org/10.1130/0016-7606(1992)104<1547:NADOCC>2.3.CO:2.
- Neuzil, C.E., 1986, Groundwater flow in low-permeability environments: Water Resources Research, v. 22, p. 1163–1195, https://doi.org/10.1029/WR022i008p01163.
- Noble, R.R.P., Gray, D.J., and Reid, N., 2011, Regional exploration for channel and playa uranium deposits in Western Australia using groundwater: Applied Geochemistry, v. 26, p. 1956–1974, https://doi.org/10.1016/j.apgeochem.2011.06.027.
- Noyes, C., Kim, J., Person, M., Ma, L., Ferguson, G., and McIntosh, J.C., 2021, A geochemical and isotopic assessment of hydraulic connectivity of a stacked aquifer system in the Lisbon Valley, Utah (USA), and critical evaluation of environmental tracers: Hydrogeology Journal, v. 29, p. 1905–1923, https://doi.org/10.1007/s10040-021-02361-9.
- Nuccio, V.F., and Condon, S.M., 1996, Burial and thermal history of the Paradox Basin, Utah and Colorado, and petroleum potential of the Middle Pennsylvanian Paradox Formation: U.S. Geological Survey Bulletin 2000-0, 41 p., https://doi.org/10.3133/b000.
- Parnell, J., 2002, Diagenesis and fluid flow in response to uplift and exhumation, in Doré, A.G., Cartwright, J.A., Stoker, M.S., Turner, J.P., and White, N., eds., Exhumation of the North Atlantic Margin: Timing, Mechanisms and Implications for Petroleum Exploration: Geological Society of London Special Publication 196, p. 433–446, https://doi.org/10.1144/GSL.SP2002.196.01.23.
- Parry, W.T., Chan, M.A., and Beitler, B., 2004, Chemical bleaching indicates episodes of fluid flow in deformation bands in sandstone: American Association of Petroleum Geologists Bulletin, v. 88, p. 175–191, https://doi.org/10.1306/09090303034.
- Parry, W.T., Forster, C.B., Evans, J.P., Bowen, B.B., and Chan, M.A., 2007, Geochemistry of CO₂ sequestration in the Jurassic Navajo Sandstone, Colorado Plateau, Utah: Environmental Geosciences, v. 14, p. 91–109, https://doi.org/10.1306/eq.07120606004.
- Pederson, J., Karlstrom, K., Sharp, W., and McIntosh, W., 2002a, Differential incision of the Grand Canyon related to Quaternary faulting—Constraints from U-series and Ar/Ar dating: Geology, v. 30, p. 739–742, https://doi.org/10.1130/0091-7613(2002)030<0739:DIOTGC>2.0.CO;2.
- Pederson, J.L., Mackley, R.D., and Eddleman, J.L., 2002b, Colorado Plateau uplift and erosion evaluated using GIS: GSA Today, v. 12, no. 8, p. 4–10, https://doi.org/10.1130/1052-5173(2002) 012<0004:CPUAEE>2.0.CO;2.
- Pederson, J.L., Anders, M.D., Rittenhour, T.M., Sharp, W.D., Gosse, J.C., and Karlstrom, K.E., 2006, Using fill terraces to understand incision rates and evolution of the Colorado River in eastern Grand Canyon, Arizona: Journal of Geophysical Research: Earth Surface, v. 111, https://doi.org/10.1029/2004JF000201.
- Pederson, J.L., Cragun, W.S., Hidy, A.J., Rittenour, T.M., and Gosse, J.C., 2013, Colorado River chronostratigraphy at Lee's Ferry, Arizona, and the Colorado Plateau bull's-eye of incision: Geology, v. 41, p. 427–430, https://doi.org/10.1130/G34051.1.
- Price, L.C., 2002, Geological and geochemical consequences of basin exhumation, and commercial implications, in Doré, A.G., Cartwright, J.A., Stoker, M.S., Turner, J.P., and White, N., eds., Exhumation of the North Atlantic Margin: Timing, Mechanisms and Implications for Petroleum Exploration: Geological Society of London Special Publication 196, p. 431, https://doi.org/10.1144/GSL.SP2002.196.01.22.
- Purser, G., Rochelle, C.A., Rushton, J., Pearce, J.M., and Wagner, D., 2014, An experimental and analogue study of iron release from red sandstones: Energy Procedia, v. 63, p. 3268–3274, https://doi.org/10.1016/j.egypro.2014.11.354.
- Ramondetta, P.J., 1982, Genesis and emplacement of oil in the San Andres Formation, northern shelf of the Midland Basin, Texas: University of Texas at Austin, Bureau of Economic Geology Report of Investigation 116, 39 p., https://doi.org/10.23867/RI0116D.
- Ranganathan, V., and Hanor, J.S., 1988, Density-driven groundwater flow near salt domes: Chemical Geology, v. 74, p. 173–188, https://doi.org/10.1016/0009-2541(88)90152-0.
- Rasmussen, L., and Rasmussen, D.L., 2009, Burial history analysis of the Pennsylvanian petroleum system in the deep Paradox Basin fold and fault belt, Colorado and Utah, *in* Houston, W.S., Wray, L.L., and Moreland, P.G., eds., The Paradox Basin Revisited: New Developments

- in Petroleum Systems and Basin Analysis: Denver, Colorado, Rocky Mountain Association of Geologists, p. 24–94.
- Reiners, P.W., 2005, Zircon (U-Th)/He thermochronometry: Reviews in Mineralogy and Geochemistry, v. 58, p. 151–179, https://doi.org/10.2138/rmg.2005.58.6.
- Reiners, P.W., Chan, M.A., and Evenson, N.S., 2014, (U-Th)/He geochronology and chemical compositions of diagenetic cement, concretions, and fracture-filling oxide minerals in Mesozoic sandstones of the Colorado Plateau: Geological Society of America Bulletin, v. 126, p. 1363–1383, https://doi.org/10.1130/B30983.1.
- Riley, K.E., Rittenour, T.M., Pederson, J.L., and Belmont, P., 2019, Erosion rates and patterns in a transient landscape, Grand Staircase, southern Utah, USA: Geology, v. 47, p. 811–814, https:// doi.org/10.1130/G45993.1.
- Rinklebe, J., and Shaheen, S.M., 2017, Redox chemistry of nickel in soils and sediments: A review: Chemosphere, v. 179, p. 265–278, https://doi.org/10.1016/j.chemosphere.2017.02.153.
- Robert, X., Moucha, R., Whipple, K., Forte, A., and Reiners, P., 2010, Cenozoic evolution of the Grand Canyon and the Colorado Plateau driven by mantle dynamics?, in Beard, L.S., Karlstrom, K.E., Young, R.A., and Billingsley, G.H., eds., CRevolution 2—Origin and Evolution of the Colorado River System, Workshop Abstracts: U.S. Geological Survey Open-File Report 2011-1210, p. 238-244.
- Rushton, J.C., Wagner, D., Pearce, J.M., Rochelle, C.A., and Purser, G., 2020, Red-bed bleaching in a CO₂ storage analogue: Insights from Entrada Sandstone fracture-hosted mineralization: Journal of Sedimentary Research, v. 90, p. 48–66, https://doi.org/10.2110/jsr.2020.4.
- Saller, A.H., and Stueber, A.M., 2018, Evolution of formation waters in the Permian Basin, United States: Late Permian evaporated seawater to Neogene meteoric water: American Association of Petroleum Geologists Bulletin, v. 102, p. 401–428, https://doi.org/10.1306/0504171612517157.
- Salvucci, G.D., and Entekhabi, D., 1995, Hillslope and climatic controls on hydrologic fluxes: Water Resources Research, v. 31, p. 1725–1739, https://doi.org/10.1029/95WR00057.
- Solum, J.G., van der Pluijm, B.A., and Peacor, D.R., 2005, Neocrystallization, fabrics and age of clay minerals from an exposure of the Moab Fault, Utah: Journal of Structural Geology, v. 27, p. 1563–1576, https://doi.org/10.1016/j.jsg.2005.05.002.
- Stone, W.J., 1983, Hydrogeology and water resources of San Juan Basin, New Mexico: New Mexico Bureau of Mines and Mineral Resources Hydrologic Report 6, 70 p., https://doi.org/10.58799/HR-6.
- Stueber, A.M., Saller, A.H., and Ishida, H., 1998, 1998, Origin, migration, and mixing of brines in the Permian Basin: Geochemical evidence from the eastern Central Basin platform, Texas: American Association of Petroleum Geologists Bulletin, v. 82, p. 1652–1672, https://doi.org/10 .1306/1D9BCB65-172D-11D7-8645000102C1865D.
- Thirumalai, K., Singh, A., and Ramesh, R., 2011, A MATLAB™ code to perform weighted linear regression with (correlated or uncorrelated) errors in bivariate data: Journal of the Geological Society of India, v. 77, p. 377–380, https://doi.org/10.1007/s12594-011-0044-1.
- Thorson, J.P., 2004, Paradox Basin sandstone-hosted copper deposits generated by two episodes of basinal fluid expulsion: Geological Society of America Abstracts with Programs, v. 36, pp. 5, p. 517
- Thorson, J.P., 2018, Paradox Basin fluids and Colorado Plateau copper, uranium, and vanadium deposits: Overview, *in* Thorson, J.P., ed., Paradox Basin Fluids and Colorado Plateau Copper, Uranium, and Vanadium Deposits Field Trip: Society of Economic Geologists Guidebook 59, p. 13–46.
- Thorson, J.P., and MacIntyre, T.J., 2005, Geology of the Cashin Mine sandstone-hosted disseminated copper deposit, Montrose County, Colorado, in Thorson, J.P., ed., Lisbon Valley Sediment-Hosted Copper Deposits and Paradox Basin Fluids Trip: Society of Economic Geologists Guidebook 37, p. 43–49, https://doi.org/10.5382/GB.37.ch4.
- Tóth, J., 1963, A theoretical analysis of groundwater flow in small drainage basins: Journal of Geophysical Research, v. 68, p. 4795–4812, https://doi.org/10.1029/JZ068i016p04795.
- Tóth, J., 1970, A conceptual model of the groundwater regime and the hydrogeologic environment: Journal of Hydrology (Amsterdam), v. 10, p. 164–176, https://doi.org/10.1016/0022-1694(70)90186-1.
- Tóth, J., 1980, Cross-formational gravity-flow of groundwater: A mechanism of the transport and accumulation of petroleum (the generalized hydraulic theory of petroleum migration), *in* Roberts, W.H., III, and Cordell, R.J., eds., Problems of Petroleum Migration: American Association of Petroleum Geologists Studies in Geology 10, p. 121–168, https://doi.org/10.1306/St10411C8.

- Tóth, J., 1999, Groundwater as a geologic agent: An overview of the causes, processes, and manifestations: Hydrogeology Journal, v. 7, p. 1–14, https://doi.org/10.1007/s100400050176.
- Trudgill, B.D., 2011, Evolution of salt structures in the northern Paradox Basin: Controls on evaporite deposition, salt wall growth and supra-salt stratigraphic architecture: Basin Research, v. 23, p. 208–238, https://doi.org/10.1111/j.1365-2117.2010.00478.x, addendum available at https://doi.org/10.1111/j.1365-2117.2011.00522.x.
- Tyne, R.L., Barry, P.H., Cheng, A., Hillegonds, D.J., Kim, J.-H., McIntosh, J.C., and Ballentine, C.J., 2022, Basin architecture controls on the chemical evolution and ⁴He distribution of groundwater in the Paradox Basin: Earth and Planetary Science Letters, v. 589, https://doi.org/10.1016/j.epsl.2022.117580.
- Uysal, I.T., and Golding, S.D., 2003, Rare earth element fractionation in authigenic illite–smectite from Late Permian clastic rocks, Bowen Basin, Australia: Implications for physico-chemical environments of fluids during illitization: Chemical Geology, v. 193, p. 167–179, https://doi .org/10.1016/S0009-2541(02)00324-8.
- Vasconcelos, P.M., Renne, P.R., Becker, T.A., and Wenk, H.-R., 1995, Mechanisms and kinetics of atmospheric, radiogenic, and nucleogenic argon release from cryptomelane during analysis: Geochimica et Cosmochimica Acta, v. 59, p. 2057–2070, https://doi.org/10.1016/0016 -7037(95)00126-3.
- von Berlepsch, T., and Haverkamp, B., 2016, Salt as a host rock for the geological repository for nuclear waste: Elements, v. 12, p. 257–262, https://doi.org/10.2113/gselements.12.4.257.
- Vrolijk, P., 1987, Tectonically driven fluid flow in the Kodiak accretionary complex, Alaska: Geology, v. 15, p. 466–469, https://doi.org/10.1130/0091-7613(1987)15
- Walker, T.R., 1967, Formation of red beds in modern and ancient deserts: Geological Society of America Bulletin, v. 78, p. 353–368, https://doi.org/10.1130/0016-7606(1967)78[353:FORBIM]2.0.CO;2.
- Whidden, K.J., Lillis, P.G., Anna, L.O., Pearson, K.M., and Dubiel, R.F., 2014, Geology and total petroleum systems of the Paradox Basin, Utah, Colorado, New Mexico, and Arizona: Mountain Geologist, v. 51, p. 119–138.
- Wigley, M., Kampman, N., Dubacq, B., and Bickle, M., 2012, Fluid-mineral reactions and trace metal mobilization in an exhumed natural CO₂ reservoir, Green River, Utah: Geology, v. 40, p. 555–558, https://doi.org/10.1130/G32946.1.
- Wilde, P., Quinby-Hunt, M.S., and Erdtmann, B.-D., 1996, The whole-rock cerium anomaly: A potential indicator of eustatic sea-level changes in shales of the anoxic facies: Sedimentary Geology, v. 101, p. 43–53, https://doi.org/10.1016/0037-0738(95)00020-8.
- Yager, R.M., McCoy, K.J., Voss, C.I., Sanford, W.E., and Winston, R.B., 2017, The role of uplift and erosion in the persistence of saline groundwater in the shallow subsurface: Geophysical Research Letters, v. 44, p. 3672–3681, https://doi.org/10.1002/2017GL072980.
- Yang, J.W., Feng, Z.H., Luo, X.R., and Chen, Y.R., 2010, Numerically quantifying the relative importance of topography and buoyancy in driving groundwater flow: Science in China Series D: Earth Sciences, v. 53, p. 64–71, https://doi.org/10.1007/s11430-009-0185-x.
- Yoshida, H., Hasegawa, H., Katsuta, N., Maruyama, I., Sirono, S., Minami, M., Asahara, Y., Nishimoto, S., Yamaguchi, Y., Ichinnorov, N., and Metcalfe, R., 2018, Fe-oxide concretions formed by interacting carbonate and acidic waters on Earth and Mars: Science Advances, v. 4, https://doi.org/10.1126/sciadv.aau0872.
- Zhang, Y., Gable, C.W., Zyvoloski, G.A., and Walter, L.M., 2009, Hydrogeochemistry and gas compositions of the Uinta Basin: A regional-scale overview: AAPG Bulletin, v. 93, p. 1087–1118, https://doi.org/10.1306/05140909004.
- Ziegler, C.L., Murray, R.W., Hovan, S.A., and Rea, D.K., 2007, Resolving eolian, volcanogenic, and authigenic components in pelagic sediment from the Pacific Ocean: Earth and Planetary Science Letters, v. 254, p. 416–432, https://doi.org/10.1016/j.epsl.2006.11.049.
- Zuo, L., Zhang, C., Falta, R.W., and Benson, S.M., 2013, Micromodel investigations of CO₂ exsolution from carbonated water in sedimentary rocks: Advances in Water Resources, v. 53, p. 188–197, https://doi.org/10.1016/j.advwatres.2012.11.004.
- Zuo, L., Ajo-Franklin, J.B., Voltolini, M., Geller, J.T., and Benson, S.M., 2017, Pore-scale multiphase flow modeling and imaging of CO₂ exsolution in sandstone: Journal of Petroleum Science Engineering, v. 155, p. 63–77, https://doi.org/10.1016/j.petrol.2016.10.011.